

Received: 31.05.2024

Accepted: 06.06.2024

Research Article

Computational Study of Potential MAO-B Inhibitors Based on 4-(3-Nitrophenyl) Thiazol-2-ylhydrazone

Moulay Ahfid El Alaouy^a, Marwa Alaqarbeh^{b,1}, Mohamed Ouabane^{a,c}, Abdelouahid Sbai^a, Hamid Maghat^a, Tahar Lakhli^a, Mohammed Bouachrine^{a,c}

^aMolecular Chemistry and Natural Substances Laboratory, Faculty of Science, University of Moulay Ismail, Meknes, Morocco

^bBasic Science Department, Prince Al Hussein bin Abdullah II Academy for Civil Protection, Al-Balqa Applied University, Al-Salt 19117, Jordan

^cChemistry-Biology Applied to the Environment URL CNRT 13, department of chemistry, Faculty of Science, My Ismail University, Meknes, Morocco.

Abstract: This study used a dataset comprising thirty-four derivatives of 4-(3-nitrophenyl) thiazol-2-ylhydrazone as selective monoamine oxidase B (h-MAO-B) inhibitors to design more effective h-MAO-B inhibitors. This was achieved by applying molecular modeling methods. Among the different field models examined, the CoMSIA/SEA model emerged as the most effective, compared to the other models ($Q^2 = 0.60$; $R^2 = 0.97$; $R^2_{test} = 0.711$; $F = 151.84$; $SEE = 0.21$; $ONC = 4$). Contour maps helped identify structural features important for inhibitory activity, leading to the design of four highly active inhibitors. The study explored the interaction between the new compounds (M1, M2, M3, and M4) and the most active molecule, No.3, using molecular docking simulations. This process revealed a positive interaction characterized by the formation of significant bonds with key protein residues such as Arg:42, Glu:58, Met:436, Tyr:398, Tyr:435, and Tyr:60. The ADMET properties of the predicted molecules (M1-M4) were generally favorable, except for molecule No.3, which retained its toxicity. Both M1 and the most active compound 3 underwent 100 ns molecular dynamics simulations, The results of these simulations indicate that the proposed molecule, M1, exhibits slightly higher structural stability compared to the most active compound, 3. This positions M1 as a promising candidate for further studies. A retrosynthesis strategy was employed to efficiently plan the synthesis of molecule M1 as a potential MAO-B inhibitor, identifying the key steps and precursors required for its realization.

Keywords: ADMET; 3D-QSAR; Molecular Modeling; hMAO-B, Thiazol-2-ylhydrazone.

[1] Introduction

Monoamine oxidase (MAO) is a class of essential enzymes involved in the degradation of neurotransmitters known as monoamines in the central nervous system. Among the various isoforms of MAO, there are two main ones: monoamine oxidase A (h-MAOA) and monoamine oxidase B (h-MAOB), which have different substrate specificities and subcellular localization. h-MAOA is primarily localized in presynaptic neurons and glial cells. It participates in the breakdown of serotonin, norepinephrine, and

dopamine [1]. Dysfunctions of h-MAOA have been associated with psychiatric disorders such as depression, anxiety, and aggression. On the other hand, h-MAOB is mainly located in astrocytes and postsynaptic neurons [2]. It is responsible for the specific degradation of dopamine, a key neurotransmitter involved in the regulation of movement, mood, motivation, and reward. Abnormalities in h-MAOB have been linked to neurodegenerative diseases such as Parkinson's disease. Understanding the mechanisms of h-MAOB and its specific role in monoamine

¹ Corresponding Authors

e-mail: marwaqarbh@hotmail.com; marwah.aqarbeh@emp.pha.edu.jo

Moulay Ahfid El Alaouy, Marwa Alaqarbeh, Mohamed Ouabane, Abdelouahid Sbai, Hamid Maghat, Tahar Lakhliifi, Mohammed Bouachrine

degradation has paved the way for major advances in drug treatment. Selective inhibitors of h-MAOA and h-MAOB have been developed and used clinically to modify levels of monoamines in the brain, thus improving symptoms associated with certain neuropsychiatric disorders [3]. h-MAOB is primarily involved in the degradation of dopamine, an important neurotransmitter for many neuronal processes. Dopamine plays a major role in the regulation of action, motivation, reward, and pleasure. h-MAOB breaks down dopamine, helping to maintain an appropriate balance of this chemical in the brain. However, dysfunction of h-MAOB can have serious consequences[4]. Excessive activity of this enzyme can lead to excessive dopamine degradation, which may be associated with neurological disorders such as Parkinson's disease. On the other hand, insufficient levels of h-MAOB may be associated with psychiatric disorders such as depression. Given its central role in dopamine degradation, h-MAOB is an important therapeutic target. Specific inhibitors of h-MAOB have been developed and used in the treatment of various neuropsychiatric disorders[5]. These inhibitors work by blocking the activity of h-MAOB, which increases dopamine levels in the brain, thereby improving symptoms associated with these disorders [6]. Considerable scholarly articles have highlighted thiazole derivatives as potent antioxidants and selective inhibitors of the hMAO-B enzyme. In their research study, Daniela Secci et al have focused on determining the quantitative structure-activity relationship of these derivatives to identify compounds with high therapeutic potential, as previously mentioned [7]. Thiazole derivatives have a wide range of applications in natural compounds, drugs, and synthetic chemicals. They demonstrate diverse pharmacological properties and can be utilized in drug design for anticancer, antimicrobial, antifungal, and anti-inflammatory agents. Derivatives of thiazoles have shown potential for reducing the activity of h-MAOB, an enzyme linked to neurological disorders. Molecular docking studies show that these compounds may effectively block h-MAOB, pointing to a strong structure-activity link that proposed new drugs [8]. The relationship between structure and activity suggests that specific thiazole ring alterations might increase inhibitory efficacy; derivatives with electron-withdrawing groups have

been discovered to have more remarkable binding affinities, which is essential for developing efficient h-MAOB inhibitors [9]. The properties and functions of these derivatives depend on their unique chemical structures. The application of computational modeling methods including 2D (2D-QSAR) and 3D (3D-QSAR) quantitative structure-activity relationship modeling molecular docking, and molecular dynamics [10].

In this study, a CoMSIA/SEA analysis was conducted on 34 compounds derived from 4-(3-nitrophenyl) thiazole-2-ylhydrazone synthesized by Daniela Secci et al. to establish a correlation between their characteristic structure and their inhibitory activity on the hMAO-B enzyme [11]. Molecular docking and ADMET studies were also used to help identify new drug candidates. Additionally, molecular dynamics simulations were carried out throughout 100 ns to assess the stability of the molecule's binding to the protein and confirm the results obtained with molecular docking. These various approaches allow for the evaluation of the structure-activity relationship of the compounds, prediction of their interaction with a molecular target, and estimation of their pharmacological potential, contributing to the identification of promising new drug candidates[12]. Therefore, research on derivatives of 4-(3-nitrophenyl) thiazole-2-ylhydrazone is an evolving field and may offer opportunities for the discovery of new drugs with improved properties and potential therapeutic applications in the treatment of Parkinson's disease.[13] However, research on these compounds should be conducted with care and caution, and any potential new agent should be thoroughly evaluated before being considered for possible clinical applications.

[2] Computational Method

2.1. Preparation of data set

In this study on selective inhibitors of human MAO-B, a dataset comprising 34 derivatives of 4-(3-nitrophenyl) thiazole-2-ylhydrazone, along with their inhibitory activities, was utilized. These data were collected from previously published studies by Daniela Secci et al [7]. Inhibitory activities were transformed into logarithms ($pIC_{50} = -\log IC_{50}$) and are presented, along with the molecular structures of the compounds, in (Table 1 and Figure 1) [14] To generate the 3D-QSAR models, the data were

Moulay Ahfid El Alaouy, Marwa Alaqarbeh, Mohamed Ouabane, Abdelouahid Sbai, Hamid Maghat, Tahar Lakhli, Mohammed Bouachrine

randomly divided into two distinct sets: a training set consisting of 27 compounds and an external test set with 7 compounds (marked with asterisks in **Table 1**). The compounds from the training set were used to develop the 3D-QSAR models, while the external test set was used as an independent group to validate the proposed models. The three-dimensional structures of the 34 compounds were generated using SYBYL-X 2.0 software.[15] Energy minimization was performed using the Tripos force field, applying Gasteiger-Hückel charges to add partial atomic charges after energy

minimization generated by the Tripos force field. The maximum number of iterations for this minimization was set to 1000, and the energy affinity value for the Powell gradient was fixed at 0.005 kcal/mol Å [16]. These preprocessing and modeling steps were undertaken to develop a reliable and robust 3D-QSAR model. The 3D-QSAR models enable the establishment of a correlation between the three-dimensional structure of the compounds and their inhibitory activity on the hMAO-B enzyme.

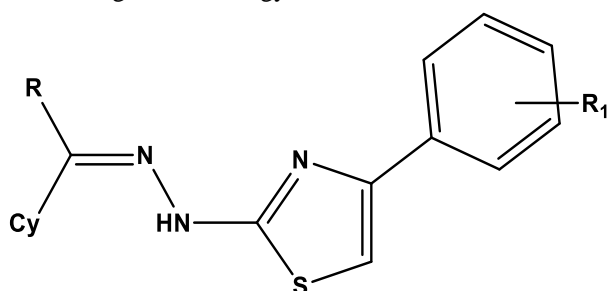
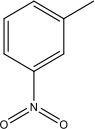
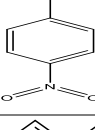
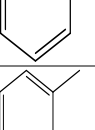
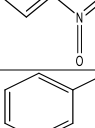
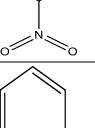
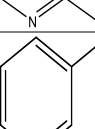
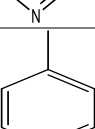
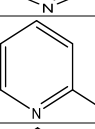
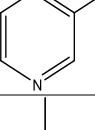
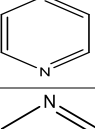
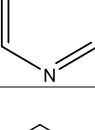
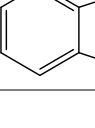


Figure 1. The chemical formula of the studied compounds.

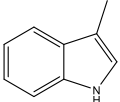
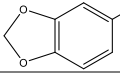
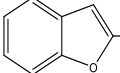
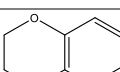
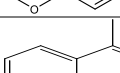
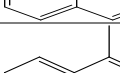
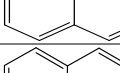
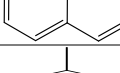
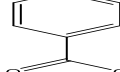
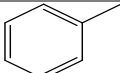
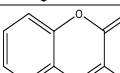
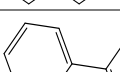
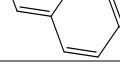
Table 1 Activities and structures of 4-(3-Nitrophenyl) thiazol-2-ylhydrazone derivatives.

N ^o	Cy	R	R ₁	IC ₅₀ (μM) hMAO-B	pIC ₅₀ hMAO-B
1		H	3-NO ₂	0.095	7.022
2		H	3-NO ₂	0.0068	8.167
3		CH ₃	3-NO ₂	0.0018	8.744
4		CH ₃	3-NO ₂	0.0025	8.602
5*		CH ₃	3-NO ₂	0.048	7.318
6		H	3-NO ₂	0.027	7.568
7		H	3-NO ₂	0.015	7.823

Moulay Ahfid El Alaouy, Marwa Alaqarbeh, Mohamed Ouabane, Abdelouahid Sbai, Hamid Maghat, Tahar Lakhli, Mohammed Bouachrine

8		H	3-NO ₂	9.11	5.04
9		H	3-NO ₂	4.63	5.334
10*		CH ₃	3-NO ₂	0.0071	8.148
11		C ₂ H ₅	3-NO ₂	0.078	7.107
12		CH ₃	3-NO ₂	0.0044	8.356
13		CH ₃	3-NO ₂	0.063	7.2
14		H	3-NO ₂	0.141	6.85
15		H	3-NO ₂	0.212	6.673
16		H	3-NO ₂	0.081	7.091
17		CH ₃	3-NO ₂	0.103	6.987
18		CH ₃	3-NO ₂	0.05	7.301
19		CH ₃	3-NO ₂	0.014	7.853
20		CH ₃	3-NO ₂	0.024	7.619
21		H	3-NO ₂	0.336	6.473

Moulay Ahfid El Alaouy, Marwa Alaqarbeh, Mohamed Ouabane, Abdelouahid Sbai, Hamid Maghat, Tahar Lakhlifi, Mohammed Bouachrine

22		CH ₃	3-NO ₂	4.52	5.344
23*		H	3-NO ₂	112	3.95
24		CH ₃	3-NO ₂	13.7	4.863
25		CH ₃	3-NO ₂	9.55	5.019
26*		H	3-NO ₂	0.045	7.346
27*		CH ₃	3-NO ₂	0.039	7.408
28		CH ₃	3-NO ₂	2.44	5.612
29		CH ₃	3-NO ₂	42.1	4.375
30			3-NO ₂	7.05	5.151
31		CH ₃	3-NO ₂	0.013	7.886
32*		CH ₃	3-NO ₂	80.5	4.094
33*		CH ₃	3-NO ₂	17.6	4.754
34		H	3-NH ₂	2.67	5.573

* Test set

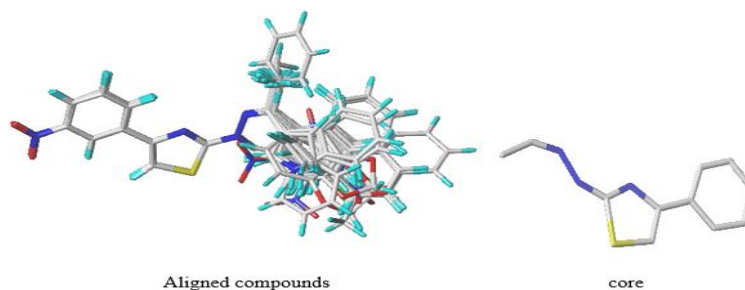


Figure 2. Alignment of the 34 molecules studied, using molecule 3 as a model.

2.2. Alignment of the inhibitors

In the study of selective inhibitors of human MAO-B, the alignment of the molecular structures of the 34 compounds is an important aspect of QSAR

(Quantitative Structure-Activity Relationship) studies.[17] This alignment enables a consistent and meaningful comparison of different compounds with varying molecular structures,

Moulay Ahfid El Alaouy, Marwa Alaqarbeh, Mohamed Ouabane, Abdelouahid Sbai, Hamid Maghat, Tahar Lakhliifi, Mohammed Bouachrine

thereby facilitating the development of reliable and predictive models. The alignment process involves adjusting the molecular structures of the compounds based on common structural elements, such as functional groups.[18] This allows for the alignment of similar properties among different compounds and the identification of the most critical molecular regions for their inhibitory activity against the target enzyme, MAO-B. In this article, the most active compound (conformation 3) was chosen as the reference for aligning other inhibitors with a common scaffold. The alignment results are presented in (Fig. 2) The 3D-QSAR models generated from the alignment help establish quantitative relationships between the 3D structural features of the compounds and their inhibitory activities.[19]

2.3. Generation of 3D-QSAR models

CoMFA (Comparative Molecular Field Analysis) and CoMSIA (Comparative Molecular Similarity Indices Analysis) are advanced 3D-QSAR methods used to analyze molecular interactions and receptor binding, playing a crucial role in the design of new biologically active compounds [20]. These techniques are essential for understanding intermolecular interactions and guiding the development of compounds with desired biological activities. Both methods use a sp^3 carbon probe with a +1 charge and a van der Waals radius of 1.52 Å to assess field energies, explore the molecular environment, and analyze electrostatic and steric interactions with target receptors. Default cutoff values greater than 30 kcal mol⁻¹ are applied to consider only the most significant interactions [21]. Gasteiger-Hückel charges are calculated for each molecule to represent atomic electrostatic properties, and fields are generated using the standard Sybyl method on a cubic grid to evaluate interactions in all directions around each compound [22]. In CoMFA, it is crucial to balance electrostatic and steric fields and precisely define the region of interest to ensure optimal model performance. Grid spacing and how indices like electrostatic and hydrophobic fields and hydrogen bond donor and acceptor properties are weighted are essential for getting an accurate CoMSIA. The width of Gaussian functions (sigma) and scaling factors must be optimized to improve the spatial distribution of similarity indices [23]. Using

contour maps to examine the fields around the molecules allows for determining the maximum biological activity within a virtual Cartesian grid. Thoroughly improving these criteria makes biological activity predictions more accurate, helps us understand how molecules interact, and makes it easier to make more biologically active compounds.[24]

2.4. Partial least squares (PLS) analysis

In this study, the Partial Least Squares (PLS) method was employed to establish a linear correlation between CoMFA and CoMSIA descriptors and biological activities. The PLS analysis involved determining the optimal number of components (NOC) and the cross-validated correlation coefficient (Q^2) using the leave-one-out (LOO) cross-validation method. LOO cross-validation allowed us to assess the predictive capacity of the model on the training data.[25] Furthermore, to evaluate the model's performance and its statistical significance, the coefficient of determination of linear regression (R^2), statistical values from the Fisher's test (F), and the Standard Error of Estimation (SEE) were calculated using the non-cross-validated method. These parameters provide insights into the quality and reliability of the correlation models.[26]

2.5. Internal and external validation of QSAR models

Internal and external validation are two crucial steps in validating QSAR models such as CoMFA and CoMSIA. Internal validation assesses the predictive capability of the model on the training data, while external validation tests its accuracy in predicting activities for new compounds not included in the training set. By employing both these validation approaches, researchers can confirm the reliability and relevance of QSAR models. The addition of Tropsha and Golbraikh's methods, as well as the Y-Randomization method, enhances the validation of QSAR models like CoMFA and CoMSIA. [27]The specific statistical criteria used by Tropsha and Golbraikh (r_m^2 , $r_m'^2$, r_0^2 , $r_0'^2$, K , and K') are employed to evaluate the predictive capacity and consistency of the models on external test sets. This confirms the reliability and generalizability of the models for predicting biological activities on new data. The Y-

Moulay Ahfid El Alaouy, Marwa Alaqarbeh, Mohamed Ouabane, Abdelouahid Sbai, Hamid Maghat, Tahar Lakhlifi, Mohammed Bouachrine

Randomization method is used to assess the significance of correlations between descriptors and activities. It helps distinguish real correlations from chance correlations, ensuring that the relationships established by the models are statistically valid and not the result of random chance. By combining these validation approaches, researchers ensure that QSAR models are robust, reliable, and capable of accurately predicting molecular interactions and inhibitory activities of the compounds under study [28]. This reinforces confidence in using these models to guide drug design and future chemical research.

2.6. Pharmacokinetic and pharmacodynamic studies

pkCSM and SwissADME are essential tools for assessing the pharmacokinetic and ADMET properties of drug candidates. pkCSM predicts drug-protein interactions and adverse effects, while SwissADME evaluates the absorption, distribution, metabolism, and excretion of small molecules. By combining these tools, researchers obtain a comprehensive assessment of drug properties and potential risks, optimizing the drug discovery process and enhancing their clinical effectiveness.[29]

2.7. Molecular docking

CB-Dock is an easy-to-use web-based molecular docking server designed for predicting specific protein binding sites and calculating cavity centers and sizes using a curvature-based approach. This remarkable software streamlines the molecular docking process by employing the well-known Autodock Vina docking software. The results obtained with CB-Dock are impressive, with a success rate of up to 70% for higher-order placements, with a root-mean-square deviation (RMSD) of less than 2 compared to placements used in X-ray crystallography. This surpasses the performance of other leading blind docking tools. The CB-Dock server is freely accessible via the official website <http://cao.labshare.cn/cb-dock/> and is a valuable tool for researchers and scientists working in drug discovery and ligand design.[30] The program only requires a protein file in PDB format and a ligand file in MOL2, MOL, or SDF format. CB-Dock analyzes the input files and converts them into pdbqt format using OpenBabel.

2.8. Molecular Dynamics Simulations

Schrödinger program was used to perform a molecular dynamics simulation study where a comprehensive set of configurations and refinements was applied to perform complex simulations after an in-depth study of molecular docking. First, we assigned bond orders, established zero-order bonds to metals, and created disulfide bonds for structural precision [31]. Excess water molecules beyond 0.00 angstroms from heteroatom groups were pruned and protonation states were generated using Epik at pH 7. For optimization, we simplified water orientations, minimized hydrogens of altered species, and performed PRPKA calculations at pH 7 for accurate protonation. During the minimization step, we removed water molecules with less than three hydrogen bonds to non-aqueous entities, achieved heavy atom convergence with an RMSD of 0.3 angstroms, and added hydrogen atoms only. The OPLS3e force field was used for intermolecular interactions [21]. The system was placed in an orthorhombic box with dimensions a=10, b=10, and c=10 to minimize volume, using a predefined SPC membrane model. Ions were recalculated and 0.15M NaCl was added to mimic physiological conditions. The simulation lasted 100 nanoseconds, with data acquired at intervals of 4.8 picoseconds for trajectory and 1.2 picoseconds for energy. Approximately 1000 frames captured the dynamics of the system under NPT conditions, with a constant temperature of 300 K and pressure of 1.01325 bar. Before simulation initiation, a relaxation process was performed to ensure a stable starting point for the molecular dynamics study [21]. After the dynamic simulation, the interaction diagram panel was used to extract data on RMSD, RMSF, Rg and other properties of the studied ligands, target proteins and complexes. This facilitated the assessment of ligand-protein interactions during the simulation and the evaluation of complex stability [17].

2.9. Retrosynthesis analysis

The retrosynthetic method stands as a fundamental strategy that provides a practical and efficient pathway for designing a synthetic sequence to create a targeted molecule. By reversing the synthetic process, starting from the target molecule and working backward to the initial reagents,

Moulay Ahfid El Alaouy, Marwa Alaqarbeh, Mohamed Ouabane, Abdelouahid Sbai, Hamid Maghat, Tahar Lakhlifi, Mohammed Bouachrine

retrosynthesis simplifies the synthesis challenge by identifying crucial steps and necessary reactions to obtain the desired compound. This approach eliminates complexity by breaking down the problem into more manageable steps, utilizing well-known functional group reactions and transformations. This methodology has been implemented through the Spaya platform (<https://www.spaya.ai>), which facilitates this process.

[3] Results and discussion

3.1. CoMSIA statistical results

For the CoMSIA analysis, various combinations of diverse domains were employed to create different models with acceptable statistical parameters ($Q^2 \geq 0.5$ and $R^2 \geq 0.6$). The results of the different components of the CoMSIA model are presented in

(Table 2). In the (CoMSIA/SEA) model, the three distinct domains produce the optimal model ($Q^2 = 0.60$; $R^2 = 0.97$; $F = 151.84$; $SEE = 0.21$; $ONC = 4$) [32]. This attests to the robustness of this model. The contributions of the electrostatic (E), steric (S), and hydrogen bond acceptor (A) domains are 41.4%, 36.9%, and 21.7%, respectively. This distribution indicates that electrostatic fields play a predominant role in enhancing inhibitory activity. Furthermore, an external validation of the CoMSIA/SEA model, conducted with test compounds, resulted in a value of 0.711, demonstrating the superior effectiveness and predictability of this model compared to others. The correlation plot between experimental inhibitory activities and predicted ones is illustrated in (Fig. 3).

Table 2. Possibilities of combining (COMSIA) fields

	Q^2	R^2	SEE	F	NOC	R^2_{Test}	Fractins	Ster	Elec	Hyd	Don	Acc
SE	0.563	0.974	0.234	125.7	4	0.69	0.42		0.578	–	–	–
SEA	0.60	0.97	0.21	151.84	4	0.71	0.369		0.414	–	–	0.217
SED	0.52	0.975	0.23	129.7	4	0.65	0.312		0.57	–	0.117	–
SHE	0.52	0.977	0.218	144.64	5	0.66	0.19		0.432	0.378	–	–
SEAD	0.581	0.982	0.194	184.16	4	0.69	0.241		0.403	–	0.089	0.267
SEADH	0.55	0.978	0.214	150.46	4	0.7	0.139		0.286	0.267	0.094	0.194
SA	0.589	0.958	0.298	76.32	5	0.55	0.452		–	–	–	0.548
SEH	0.526	0.977	0.218	144.64	5	0.66	0.19		0.432	0.378	–	–
DA	0.579	0.87	0.52	22.4	6	0.56	–		–	–	0.183	0.817
A	0.53	0.816	0.624	14.78	6	0.63	–		–	–	–	1
SHDA	0.52	0.967	0.263	98.656	6	0.54	0.179			0.385	0.11	0.326
SEHA	0.552	0.979	0.21	156.78	4	0.68	0.157		0.311	0.314	–	0.219
SEHD	0.522	0.975	0.23	130.6	4	0.69	0.227		0.352	0.329	0.091	

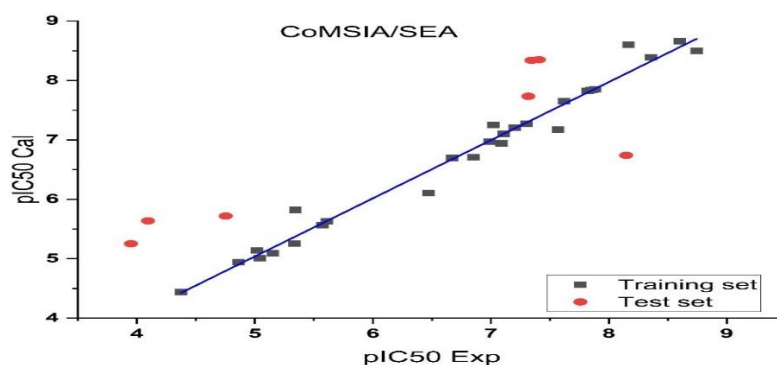


Figure 3. Plot of experimental activity versus predicted activity by the optimal CoMSIA/SEA model

3.2. Validation of CoMSIA/SEA model

The Y-randomization test is employed to assess the robustness of CoMSIA/SEA and to avoid chance associations between descriptors and biological

activity. Ten tests were conducted using randomization methods, as presented in (Table 3). The results of the Y-randomization test demonstrated Q^2 and R^2 values higher than those

Moulay Ahfid El Alaouy, Marwa Alaqarbeh, Mohamed Ouabane, Abdelouahid Sbai, Hamid Maghat, Tahar Lakhlifi, Mohammed Bouachrine

of the studied model, indicating that the CoMFA/SEA model was not obtained randomly. This observation attests to the strength and credibility of the established model. [33] Furthermore, the external validation approaches of Golbraikh and Tropsha were employed to validate the chosen CoMSA/SEA

model. The results listed in (Table 4) demonstrate that the model met all external validation criteria, confirming its robustness and predictive power.[34] The table labeled as (Table 5) displays the comparative outcomes of actual and predicted activities obtained from the COMSIA/SEA models designed for hMAO-B inhibitors.

Table 3. R²_{train} and Q² LOO values after the Y-randomization experiments.

Model	R	R ²	Q ²
Random 1	0.16	0.025	-0.132
Random 2	0.057	0.003	-0.2295
Random 3	0.096	0.009	-0.162
Random 4	0.120	0.014	-0.176
Random 5	0.388	0.15	-0.017
Random 6	0.273	0.074	-0.201
Random 7	0.157	0.024	-0.183
Random 8	0.183	0.033	-0.104
Random 9	0.161	0.025	-0.234
Random 10	0.174	0.03	-0.134
Random Models Parameters			
Average	0.177	0.039	-0.157

Table 4. provides the statistical criteria utilized to validate the CoMSIA/SEA model.

Parameter	Equation	COMSIA/SEA	Validation Criteria
R ² (test)	$R_{test}^2 = 1 - \frac{\sum(Y_{pred(test)} - Y_{obs(test)})^2}{\sum(Y_{obs(test)} - \bar{Y}_{obs(test)})^2}$	0.71	>0.60
r ₀ ²	$r_0^2 = 1 - \frac{\sum(Y_{test(pred)} - kY_{test(pred)})^2}{\sum(Y_{test(pred)} - \bar{Y}_{test(pred)})^2}$	0.73	>0.50
r' ₀ ²	$r_0'^2 = 1 - \frac{\sum(Y_{test} - kY_{test})^2}{\sum(Y_{test} - \bar{Y}_{test})^2}$	0.912	>0.50
\bar{r}_0^2	$\frac{ r_0^2 + r_0'^2 }{2}$	0.821	< 0.50
Δr_0^2	$ r_0^2 - r_0'^2 $	0.232	< 0.30
$\frac{(r^2 - r_0^2)}{r^2}$	$\frac{(r^2 - r_0^2)}{r^2}$	-0.074	< 0.10
$\frac{(r^2 - r_0'^2)}{r^2}$	$\frac{(r^2 - r_0'^2)}{r^2}$	-0.341	< 0.10
K	$k = \frac{\sum(Y_{obs} \times Y_{pred})^2}{\sum(Y_{pred})^2}$	0.908	0.85 ≤ K ≤ 1.15
K'	$k' = \frac{\sum(Y_{obs} \times Y_{pred})^2}{\sum(Y_{obs})^2}$	1.077	0.85 ≤ K' ≤ 1.15

Table 5. Experimental and predicted pIC₅₀ of the CoMSIA/SEA models

Moulay Ahfid El Alaouy, Marwa Alaqarbeh, Mohamed Ouabane, Abdelouahid Sbai, Hamid Maghat, Tahar Lakhlifi, Mohammed Bouachrine

N°	pIC ₅₀ (M)	CoMSIA/SEA		N°	pIC ₅₀ (M)	CoMSIA/SEA	
		Predicted	residuals			Predicted	Residuals
1	7.022	7.251	-0.229	18	7.301	7.272	0.029
2	8.167	8.603	-0.436	19	7.853	7.838	0.015
3	8.744	8.497	0.247	20	7.619	7.65	-0.031
4	8.602	8.66	-0.058	21	6.473	6.104	0.369
5*	7.318	7.734	-0.416	22	5.344	5.822	-0.478
6	7.568	7.176	0.392	23*	3.95	5.252	-1.302
7	7.823	7.824	-0.001	24	4.863	4.941	-0.078
8	5.04	5.008	0.032	25	5.019	5.14	-0.121
9	5.334	5.257	0.077	26*	7.346	8.339	-0.993
10*	8.148	6.74	1.408	27*	7.408	8.349	-0.941
11	7.107	7.104	0.003	28	5.612	5.631	-0.019
12	8.356	8.39	-0.034	29	4.375	4.437	-0.062
13	7.2	7.204	-0.004	30	5.151	5.091	0.06
14	6.85	6.706	0.144	31	7.886	7.853	0.033
15	6.673	6.697	-0.024	32*	4.094	5.638	-1.544
16	7.091	6.941	0.15	33*	4.754	5.718	-0.964
17	6.987	6.97	0.017	34	5.573	5.567	0.006

* Test set

The results of the Y-randomization test demonstrated Q2 and R2 values higher than those of the studied model, indicating that the CoMFA/SEA model was not obtained

3.3. Graphical interpretation of the best CoMSIA/SEA model

The graphical representation of field contours for the chosen CoMSIA/S+E+A model is displayed in (Fig. 4). The distributions of the steric field, electrostatic field, and hydrogen bond acceptor field of CoMSIA are shown in Figures (a), (b), and (c), respectively.[35]

Steric Field (a): The green and yellow contours indicate that the presence of a bulky group is advantageous for increasing activity, while it is unfavorable for decreasing it. The green contour adjacent to the substituent -R suggests that the incorporation of bulky substituents could enhance biochemical activity at this location. This also explains the higher activity of compound 3 bearing the -CH₃ radical compared to compound 2 with the -H radical. Similarly, compound 10 with the -CH₃ radical is more active than compound 6 containing the -H radical.

Electrostatic Field (b): Electrostatic contours, where blue areas indicate a preference for positive charges and red areas for negative charges. We identified a red contour near the ring, suggesting that the presence of mesomeric electron-attracting groups at this location (ortho position) is favorable

for improving biological activity. This is supported by the observation that compound 12 (pIC₅₀ = 8.356) with the -NO₂ group in the ortho position exhibits higher activity than compound 13 (pIC₅₀ = 7.2) with the -NO₂ group in the para position[36]. Hydrogen Bond Acceptor Field (c): The magenta contours (80% contribution) delineate areas favorable to hydrogen bond acceptors, while the red regions (20% contribution) indicate undesirable acceptors. We observed a magenta contour near the thiophene ring, suggesting that an increase in compound activity occurs in the presence of a hydrogen bond acceptor group. However, the red contour demonstrates that the presence of a hydrogen bond acceptor has an unfavorable effect on compound activity[37].

3.4. Design of new inhibitors

The primary objective of this study is to identify new MAO-B inhibitors using CoMSIA/SEA contour maps. These maps help identify specific target regions that can be modified to enhance inhibitory activity, measured in terms of pIC₅₀[38]. In this endeavor, four new derivatives of 4-(3-nitrophenyl) thiazole-2-ylhydrazone were synthesized and evaluated. The results showed that these derivatives exhibit significantly higher inhibitory activity compared to the parent compound, referred to as "compound 3."

The data obtained are listed in (Table 6), where the predicted pIC₅₀ values, total docking scores, and

Moulay Ahfid El Alaouy, Marwa Alaqarbeh, Mohamed Ouabane, Abdelouahid Sbai, Hamid Maghat, Tahar Lakhlifi, Mohammed Bouachrine

chemical structures of the new compounds are detailed [39]. These pieces of information highlight the correlation between the structural features of the new compounds and their enhanced inhibitory

activity [40]. This suggests that the modifications made to the molecular structures have had a positive effect on their affinity for the MAO-B target [41].

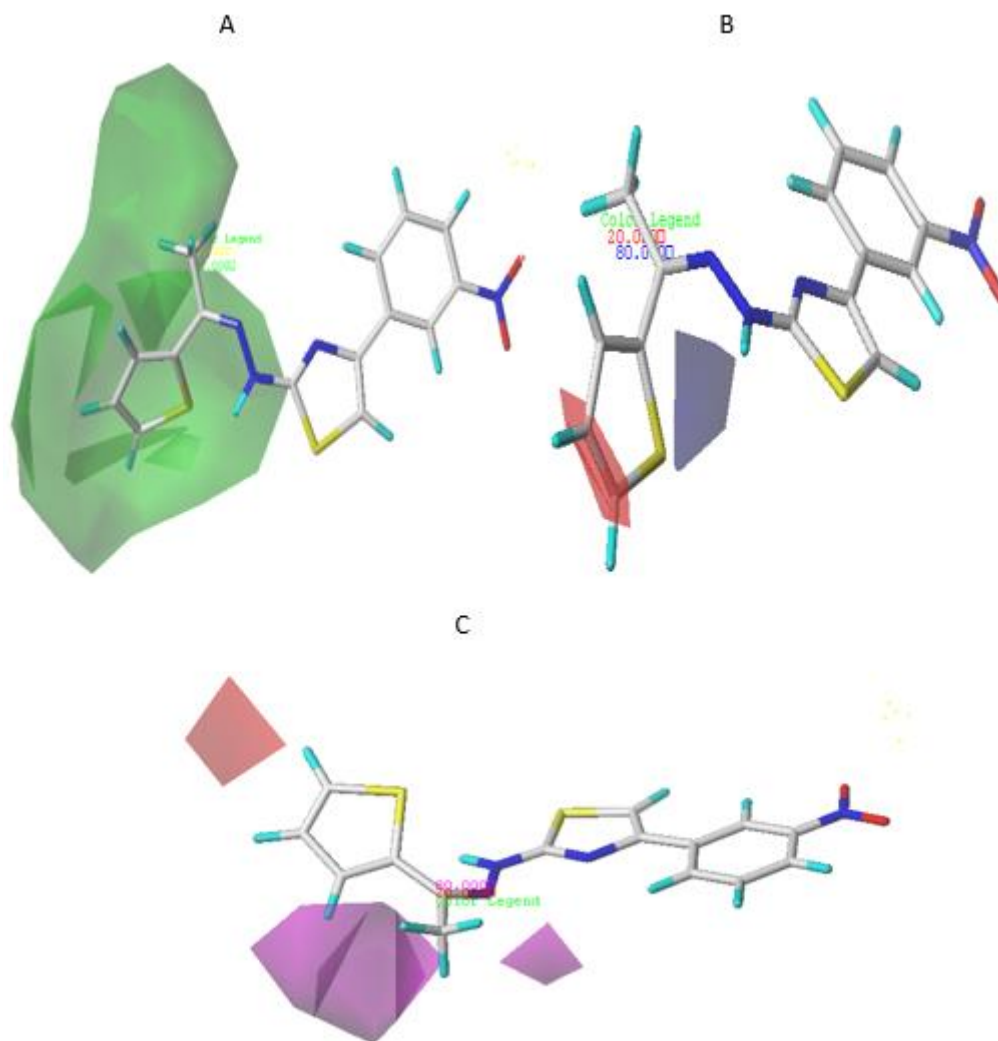
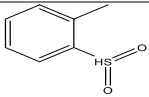
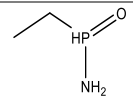
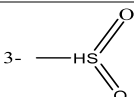
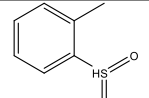
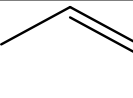
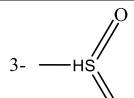


Figure 4. contour maps derived from the most refined CoMSIA/SEA model: (A) steric field, (B) electrostatic field and (C) hydrogen bond acceptor field.

Table 6. shows the structures of the newly designed compounds and their predicted pIC50s.

N°	Structure			Predicted pIC50 CoMSIA (SEA)
	Cy	R	R1	
Comp 3		CH ₃	3-NO ₂	8.55
M1			3-	9.98
M2			3-	9.67

Moulay Ahfid El Alaouy, Marwa Alaqarbeh, Mohamed Ouabane, Abdelouahid Sbai, Hamid Maghat, Tahar Lakhlifi, Mohammed Bouachrine

M3				9.60
M4				8.58

3.5. In silico ADEMT and drug-like prediction

The prediction of ADMET characteristics is of crucial importance to anticipate potential issues during later stages of clinical therapies. Therefore, the pkCSM and SwissADME tools were used to predict the ADMET properties of the new derivatives of 4-(3-nitrophenyl)thiazole-2-ylhydrazone. (Table 7) illustrates the Lipinski properties profile for the new molecules under consideration, while (Table 8) details the predicted in silico ADMET properties. In parallel, (Table 9) presents the toxicity evaluation results for the new molecules M1, M2, M3, M4, and 3 using four parameters.[42]

According to Lipinski's Rule of Five, a compound with a logP value less than 5, a molecular weight (MW) of 500 Da or less, fewer than 10 hydrogen bond acceptors (HBA), and fewer than 5 hydrogen bond donors (HBD) is considered to have good absorption properties (Rule of Five Criteria). (Table 7) demonstrates that the proposed molecules, as well as the most active molecule, compound 3, meet these criteria by having a logP value less than 5, an MW less than 500 Da, an HBA count less than 10, and an HBD count less than 5. Additionally, the number of rotatable bonds (NROTB) is less than 10, indicating that these compounds have better absorption and bioavailability capabilities.

As revealed in (Table 8), all compounds exhibit absorption rates exceeding 80% in the human intestine, indicating high intestinal absorption, while values below 30% signify low absorption. Cytochrome P450 is an essential enzymatic system for drug metabolism in the liver, with CYP3A4 being one of its major variants. All the considered molecules act as inhibitors and substrates of CYP3A4, except for the most active molecule, compound 3. Furthermore, their synthetic accessibility scores range from 3.49 to 4.27, indicating ease of synthesis.[43]

(Table 9) presents the results of toxicity assessment using four parameters. The AMES test confirmed the absence of mutagenic and carcinogenic properties in all newly designed candidates, except for the reference compound 3, which remains toxic. Additionally, the acute toxicity (LD50) of the compounds ranged from 2.292 to 3.04 mol/kg, while the chronic toxicity (LOAEL) of the compounds ranged from 1.239 to 2.047 mg/kg of body weight per day. Furthermore, none of the newly synthesized compounds cause skin sensitization. Considering these results, it is possible to conclude that most candidates do not pose potential toxic concerns, except for compound 3.

Table 7 In silico ADMET properties of the proposed new compounds and reference compound 3.

	3	M1	M2	M3	M4
Intestinal absorption (human) Numeric (% Absorbed)	86.426	95.022	89.671	81.681	82.039
CYP2D6 substrate	NO	NO	NO	NO	NO
CYP3A4 substrate	YES	YES	YES	YES	YES
CYP1A2 inhibitor	YES	NO	NO	NO	YES
CYP2C19 inhibitor	YES	YES	YES	YES	YES
CYP2C9 inhibitor	YES	YES	YES	YES	YES
CYP2D6 inhibitor	NO	YES	NO	NO	NO
CYP3A4 inhibitor	NO	YES	YES	YES	YES
Total Clearance	0.313	0.549	0.1	0.16	0.132
Synthetic Accessibility	3.98	3.73	4.27	4.24	3.49

Moulay Ahfid El Alaouy, Marwa Alaqarbeh, Mohamed Ouabane, Abdelouahid Sbai, Hamid Maghat, Tahar Lakhlifi, Mohammed Bouachrine

Table 8. Lipinski characteristics of the recently developed M1-M4 compounds and the reference compound 3.

	3	M1	M2	M3	M4
Lipinski	YES	YES	YES	YES	YES
Log P	4.61	4.95	2.8282	2	2.753
nHBD	1	1	3	4	3
nHBA	7	9	9	9	8
Nrotb	5	8	8	8	7
MR	96.53	116.95	116.70	116.00	108.63
MW	344.42	428.49	482.42	484.521	433.536

Table 9. Predicting the toxicity of newly developed compounds and the reference compound 3.

Comp N°	AMES Toxicity Yes/No	Oral Rat Acute Toxicity (LD ₅₀) mol/Kg	Oral Rat Chronic Toxicity (LOAEL) Log mg/kg_ bw/day	Skin Sensitisation Yes/No
3	YES	2.889	1.398	NO
M1	NO	3.04	1.239	NO
M2	NO	2.317	2.047	NO
M3	NO	2.292	1.962	NO
M4	NO	2.437	1.968	NO

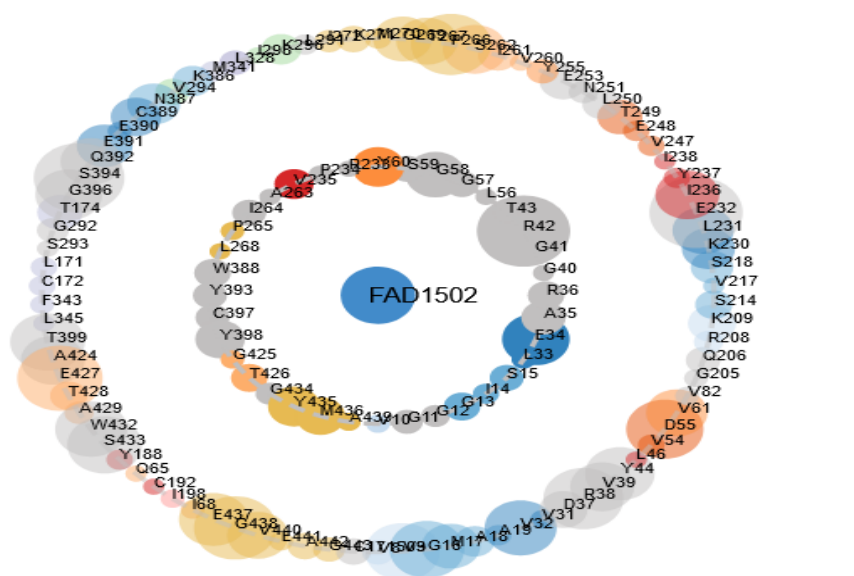


Figure 5. Graph of protein-ligand interactions in asteroids.

3.6. Molecular docking results

To gain a comprehensive understanding of the quantitative relationship between the molecular structure and its activity, as indicated by the 3D-QSAR model, it is imperative to grasp the principles of ligand-receptor binding, a process often studied through molecular docking. In this study, the researchers utilized an online web service called the Atlas of Protein Communications.

Additionally, crucial interactions involving specific amino acids were discerned using graphical representations in the form of ligand and residue "asteroid" plots (please refer to (Fig. 5)). These visualizations highlighted larger circles along the main chain, corresponding to residues like Arg:42, Glu:34, Glu:58, Met:436, Tyr:398, Tyr:435, Tyr:60, and Arg:41, underscoring the significant roles played by these amino acids in the binding

Moulay Ahfid El Alaouy, Marwa Alaqarbeh, Mohamed Ouabane, Abdelouahid Sbai, Hamid Maghat, Tahar Lakhlifi, Mohammed Bouachrine

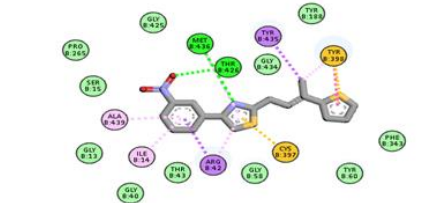
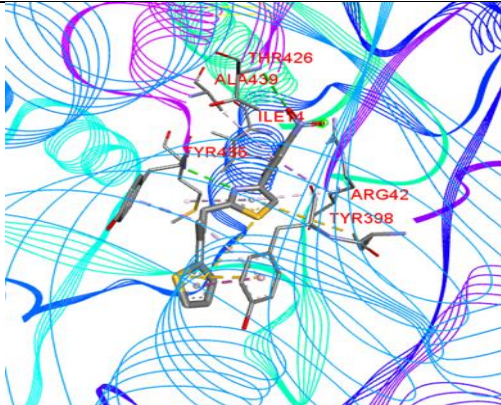
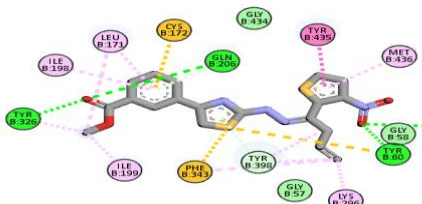
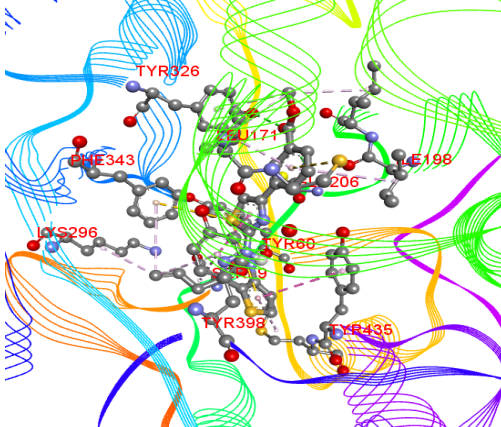
process. This insight was instrumental in assessing the compound's activity and confirming the success of the molecular docking procedure[44].

A molecular docking study was carried out to validate the 3D-QSAR method by examining the interactions between the ligand variants (M1 to M4) and the hMAO-B receptor (PDB: 2V60) [45]. Table 10 depicts the 2D and 3D interactions, while Table 11 summarises the binding energies of these molecules.

The most active molecule, compound 3, has several critical interactions with the hMAO-B receptor, including hydrogen bonds between the nitro group and Thr426, and between the thiazole group and Met436, a Pi-Sulphur interaction of the thiophene group with Tyr398, a Pi-Sigma interaction of the

methyl group with Tyr435, and alkyl interactions between the benzene group and residues Ala439 and Ile14. In addition, the thiazole and benzene rings form Pi-Alkyl interactions with Arg42 and Cys397[46]. These interactions are crucial for the efficacy of compound 3 as an hMAO-B inhibitor, as shown by a binding score of -9 kcal/mol. For compound M1, the main interactions include hydrogen bonds of the nitro group with Tyr60 and Ser59 and the methyl acetate group with Gln206 and Tyr326. Pi-alkyl interactions of the 1-butane group with Lys296 and Tyr398 and of the thiophene ring with Met436 are also notable. In addition, the thiophene group forms a T-shaped Pi-Pi interaction with Tyr435, while thiazole forms a stacked Pi-Pi interaction with Phe343 as Hydrogen bonding.

Table 10. Chemical interactions depicted for the proposed compounds and the active compound (3) at the receptor binding sites (PDB ID: 2V60) in 2D and 3D Docking.

N°	2D View	3D View
3	 <p data-bbox="414 1220 718 1321"> Interactions ■ van der Waals ■ Conventional Hydrogen Bond ■ Pi-Sigma ■ Pi-Sulfur ■ Pi-Pi Stacked ■ Pi-Alkyl </p>	
M1	 <p data-bbox="414 1657 718 1758"> Interactions ■ van der Waals ■ Conventional Hydrogen Bond ■ Pi-Donor Hydrogen Bond ■ Pi-Sulfur ■ Pi-Pi Stacked ■ Pi-Pi T-shaped ■ Alkyl ■ Pi-Alkyl </p>	

Moulay Ahfid El Alaouy, Marwa Alaqarbeh, Mohamed Ouabane, Abdelouahid Sbai, Hamid Maghat, Tahar Lakhli, Mohammed Bouachrine

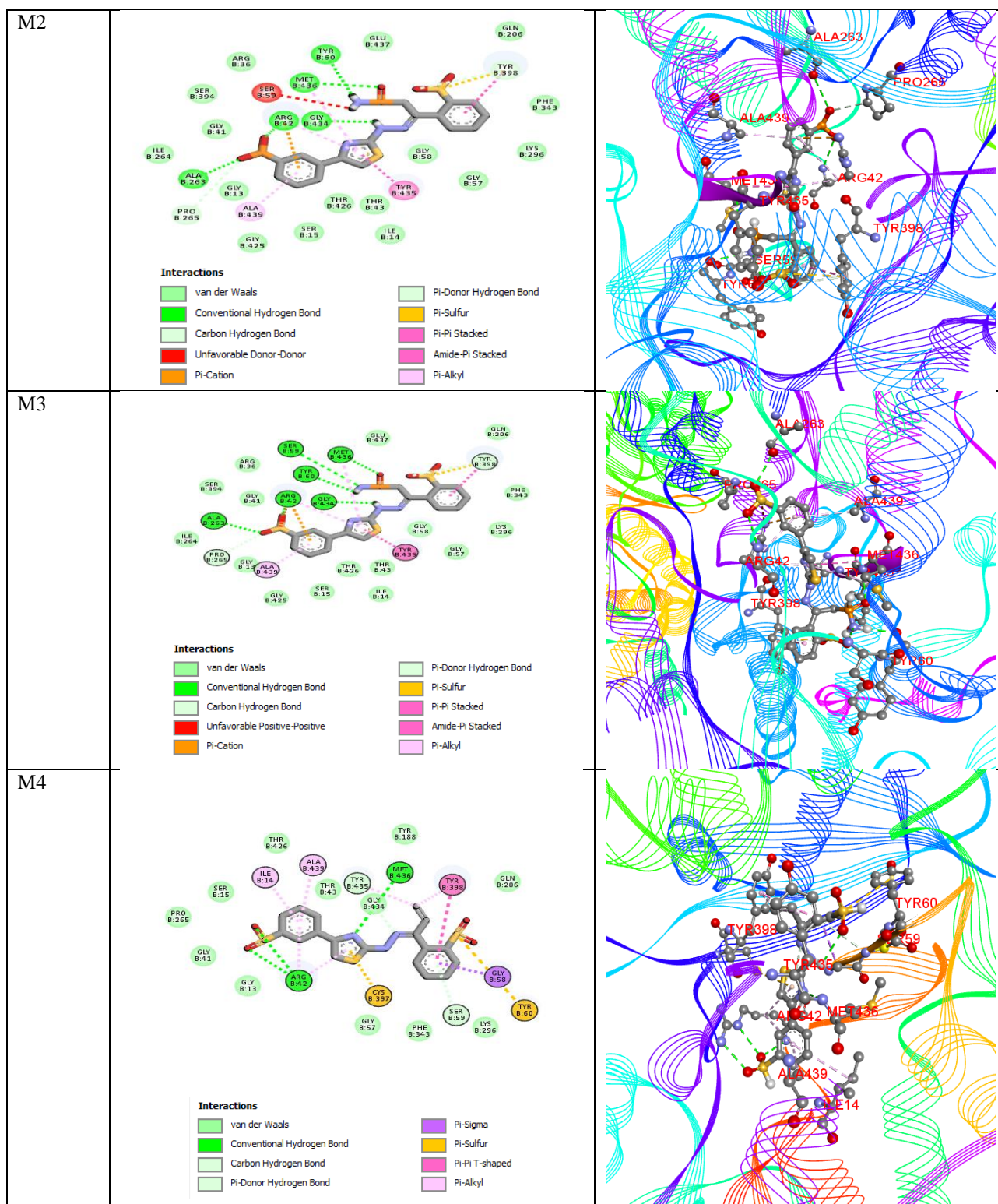


Table 11. Molecular docking score for newly discovered compounds using the CoMSIA/SEA model.

N ^o	Affinity (kcal/mol)
3	-9
M1	-9.7
M2	-10

Moulay Ahfid El Alaouy, Marwa Alaqarbeh, Mohamed Ouabane, Abdelouahid Sbai, Hamid Maghat, Tahar Lakhlifi, Mohammed Bouachrine

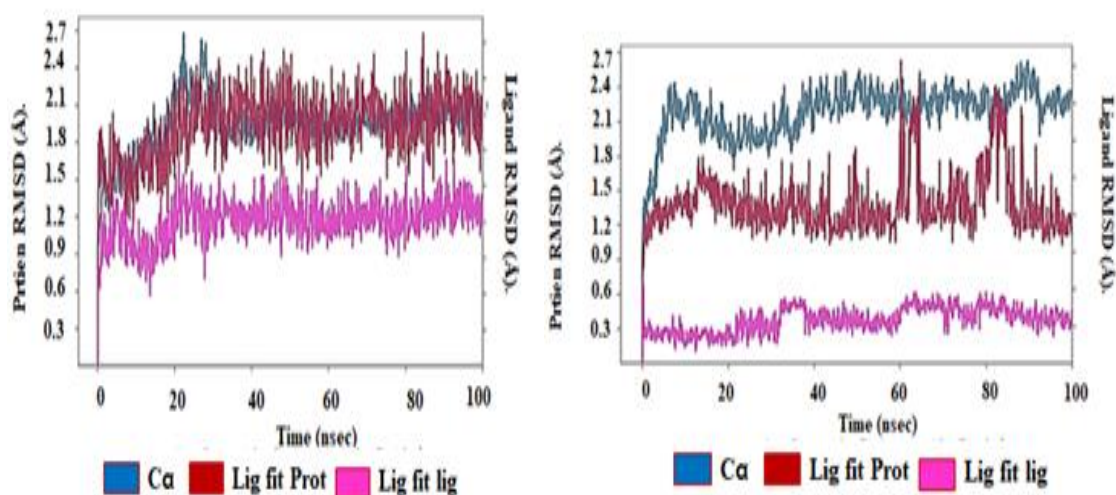
M3	-9.5
M4	-9.2

3.7. Molecular dynamics

The results from molecular dynamics simulations (Fig. 6) of the proposed M1 molecule provided crucial insights into the root mean square deviation (RMSD) of the ligand, protein, and protein-ligand complex. The RMSD values were employed to assess stability and conformational variations throughout dynamic simulation. They exhibited a maximum RMSD of 1.5 Å for the ligand, 2.7 Å for the protein, and 2.7 Å for the complex, with a minimum RMSD of 0.6 Å for the ligand, 1.2 Å for the protein, and 1.2 Å for the complex. After 25 nanoseconds, the RMSD fluctuations converged to approximately 1 Å for the ligand and 2.1 Å for the protein and the complex, indicating a certain degree of structural equilibrium. During this period, the ligand altered its conformation and position within the protein's active site, facilitating crucial interactions with amino acids, attributed to the presence of electron-withdrawing groups (NO₂) and the orientation of CH₃O- in the Ester

function[49]. The combined RMSD between the protein alone and the protein-ligand complex suggests a stable and strong binding, with minimal major structural changes.

In the case of the most active molecule 3, a maximum RMSD of 1.2 Å for the ligand, 4.7 Å for the protein, and 4.8 Å for the complex was observed, with a minimum RMSD of 0.3 Å for the ligand, 3 Å for the protein, and 1.8 Å for the complex. Over 100 nanoseconds, the ligand underwent conformational changes and/or altered its position within the protein's active site, facilitating critical interactions with amino acids, attributed to the presence of electron-withdrawing groups (NO₂) and a conjugated main chain system[50]. This justifies the conformational changes observed in the most active molecule, although typically, no stable conformation was maintained throughout the dynamic simulation period.

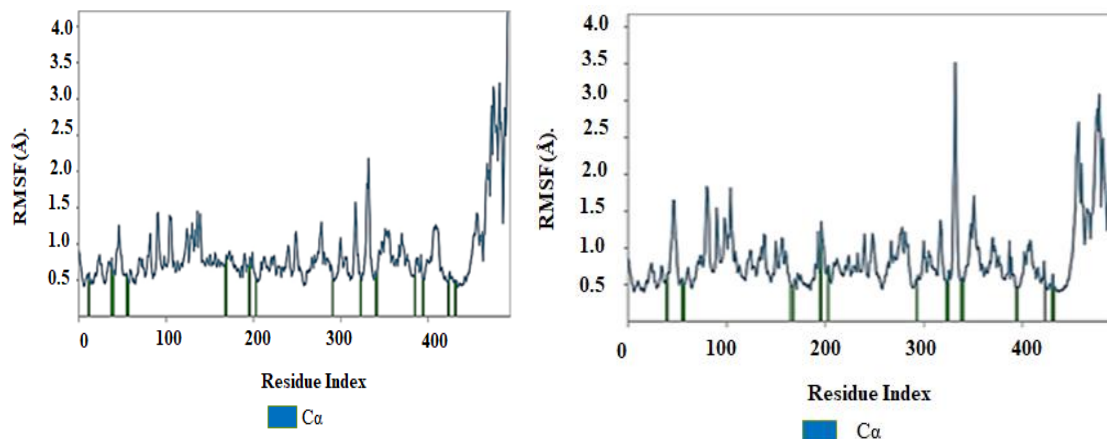


Suggested molecules M1

More-active molecules 3

Figure 6. RMSD of ligands, protein (C-alpha) and the complex

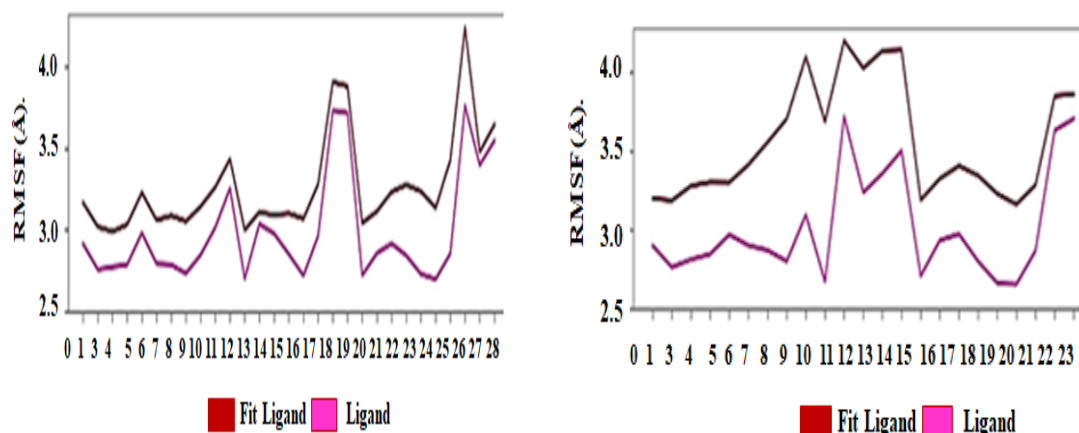
Moulay Ahfid El Alaouy, Marwa Alaqarbeh, Mohamed Ouabane, Abdelouahid Sbai, Hamid Maghat, Tahar Lakhli, Mohammed Bouachrine



Suggested molecules M1

More-active molecules 3

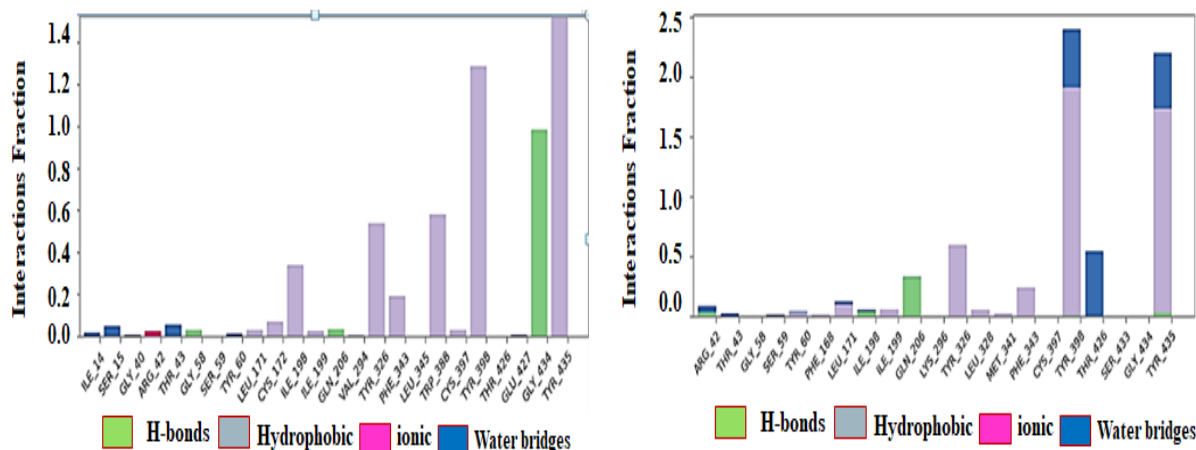
Figure 7. RMSF of therapeutic target amino acids



Suggested molecules M1

More-active molecules 3

Figure 8. RMSF of ligands with and without the influence of amino acids



Suggested molecules M1

More-active molecules 3

Figure 9. Type and interaction fractions of amino acids in contact with ligands.

In order to assess the vibrations of amino acids relative to their initial conformation, the RMSF (Root Mean Square Fluctuation) value of the target

receptor was considered and measured by tracking the variation in $C\alpha$ atoms of the peptide chain. The RMSF values of the receptor protein revealed

Moulay Ahfid El Alaouy, Marwa Alaqarbeh, Mohamed Ouabane, Abdelouahid Sbai, Hamid Maghat, Tahar Lakhliifi, Mohammed Bouachrine

fluctuations ranging from 0.5 to 2 Å, with the exception of the C-terminal amino acids, whether in the presence of the most active molecule or the proposed one. Upon analysis, it was found that the RMSF values for the complex system were lower for active amino acids. When comparing the number of amino acids involved in conventional hydrogen bond interactions between the proposed M1 molecule and the most active one 3, it became evident that our proposal formed more interactions throughout the dynamic simulation. The fluctuations of amino acids and their interactions with the ligands are depicted in (Fig. 7).

Interpreting the RMSF (Root Mean Square Fluctuation) of the ligand with and without the protein's influence can provide crucial insights into the ligand's flexibility and stability in the presence of the protein. The fluctuation of carbon atom number 11, sp² hybridized, is approximately 1 Å, the fluctuation of the two oxygen atoms, numbers 18 and 19, from the nitro group is around 1.5 Å, and the fluctuation of oxygen atom number 27, sp³ hybridized from the ester function, is about 2 Å. Conversely, the fluctuations of the other atoms in the proposed M1 molecule are less than 1 Å in the presence of the protein and less than 0.5 Å without protein influence. This range of difference suggests that the ligand adopts a more stable and protein-interaction-favorable conformation.

As for the most active 3 molecule, the fluctuation of carbon atom number 9 from the methyl group is approximately 0.5 Å without protein influence and around 1.5 Å in the presence of the protein. The fluctuation of carbon atom number 11 from the 5-membered ring is about 1.2 Å and 1.6 Å with and without protein influence, respectively. The fluctuation of nitrogen atom number 14 from the 5-membered ring is approximately 1 Å without protein effect and roughly 1.6 Å with protein effect. The fluctuation of two oxygen atoms from the nitro group is about 1.3 Å and 1.45 Å with protein influence and without protein influence, respectively. The other fluctuations of atoms in the most active molecule are below 1.1 Å.

In general, atomic vibrations of the added substitutions, as indicated by the analysis of contour maps from the CoMSIA prediction model, formed significant interactions in the molecular docking analysis and adhere to the maximum fluctuation thresholds, as demonstrated by the RMSF analysis

over 100 nanoseconds. These fluctuations are illustrated in (Fig. 8).

The proposed M1 molecule forms various types of interactions with the therapeutic target, such as three H-Bond interactions with GLU: 427, GLN: 206, and GLY: 58, as well as hydrophobic interactions with amino acids TYR: 435, TYR: 398, TPR: 388, TPR: 326, and ILE: 198, some of which have a very high fraction while others are less intense. Additionally, ionic interactions are observed with ARG: 42, along with water bridge interactions with THR: 43, SER: 15, and ILE: 14 during the dynamic simulation.

Regarding the most active molecule 3, it exhibits low-intensity H-Bond interactions with amino acids GLN: 206, ILE: 198, and ARG: 42, although these interactions are relatively weak. Two significant and noteworthy interactions are formed between this molecule and the therapeutic target, characterized by more intense hydrophobic interactions, along with water bridge interactions.

In general, upon analyzing interactions with amino acids during the dynamic simulation, it is evident that the proposed molecule outperforms the most active molecule. These interactions are depicted in (Fig. 9).

In order to track these ligand-protein interactions, a detailed study of these interactions over 100 nanoseconds was performed to confirm amino acid contacts with the studied ligands. It was observed that the number of these contacts varied from 3 to 9 bonds for the proposed M1 molecule and sometimes up to 12 bonds for the most active molecule. However, during the dynamic simulations the amino acids TYR: 435, GLY: 434, TYR: 398, TRP: 388, and TYR: 326 remained in contact with the proposed molecule, while the contact between the most active molecule 3 and the therapeutic target was not continuous compared to the contact of the proposed molecule. This indicates that the interactions of our proposal are stronger than those of the base's most active molecule. The number of ligand-protein contacts and the continuity of interactions with the therapeutic target are shown in (Fig. 10).

Molecular dynamics results show the percentages of different secondary structures in the two studied complexes, the first being the proposed M1 molecule with the protein and the second being the most active molecule 3 with the protein. Secondary

Moulay Ahfid El Alaouy, Marwa Alaqarbeh, Mohamed Ouabane, Abdelouahid Sbai, Hamid Maghat, Tahar Lakhlifi, Mohammed Bouachrine

structures generally include helices (alpha helices) and strands (beta sheets), which are important elements of protein conformation.

For complex M1 we observe about 25.30% helices, 17.56% strands and a total of 42.86% secondary

structures. Conversely, for complex 3, we observe a slightly higher percentage with about 25.87% helices, 18.11% strands and a total of 43.97% secondary structures.

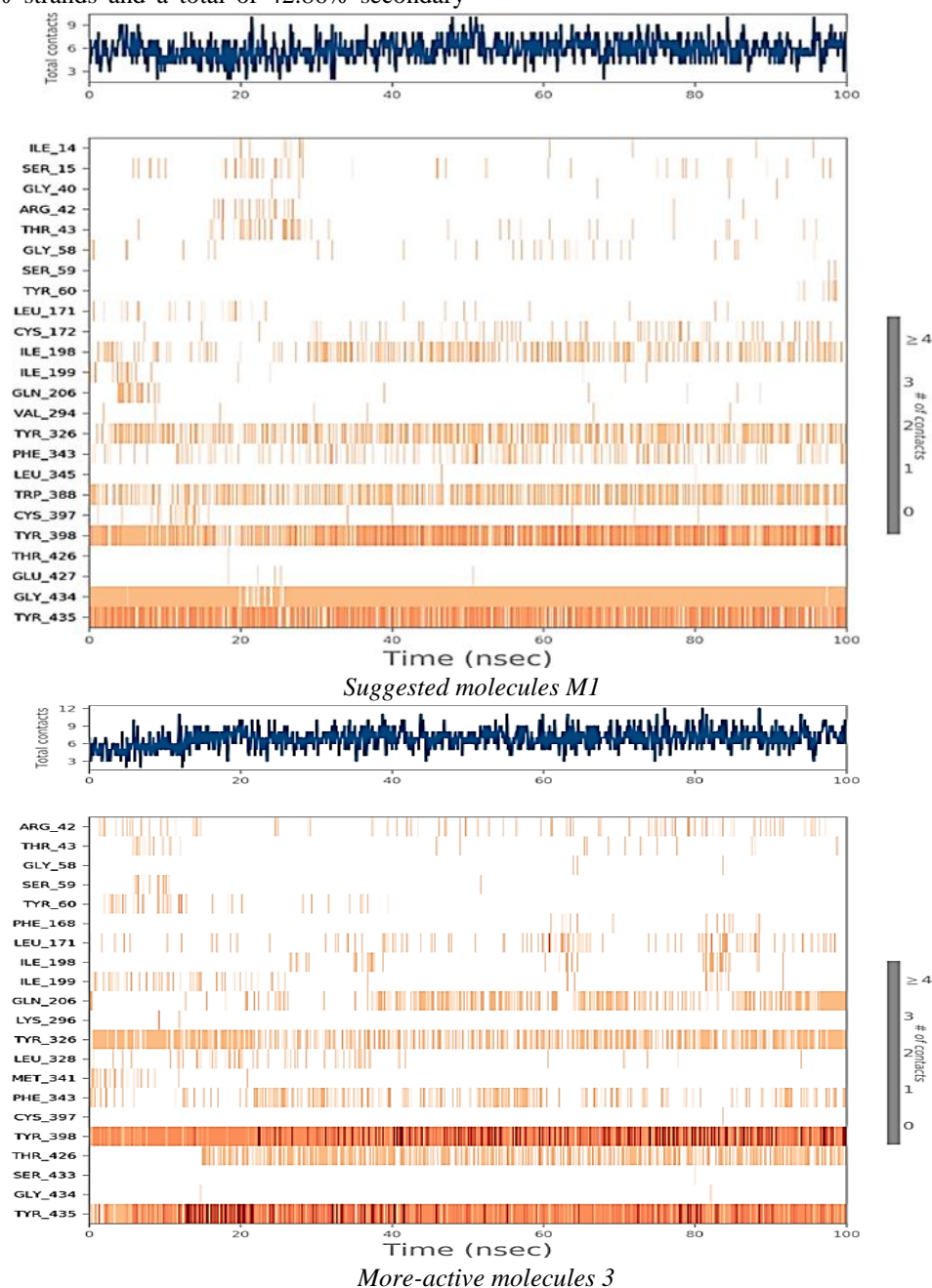


Figure 10. Number of amino acid contacts over time in the dynamic simulation

The information presented in (Fig. 11) suggests that the two complexes have relatively comparable secondary structure compositions, albeit with a slight advantage in favour of complex M1. Nevertheless, these differences remain relatively subtle, suggesting that the two molecules exhibit

similarities in their overall conformation and structural behavior during molecular dynamics. It should be noted that these results could have implications for the stability and functionality of the molecules, but a more comprehensive analysis is required to fully grasp the influence of these

Moulay Ahfid El Alaouy, Marwa Alaqarbeh, Mohamed Ouabane, Abdelouahid Sbai, Hamid Maghat, Tahar Lakhli, Mohammed Bouachrine

variations in secondary structure on their respective biological behaviors[51].

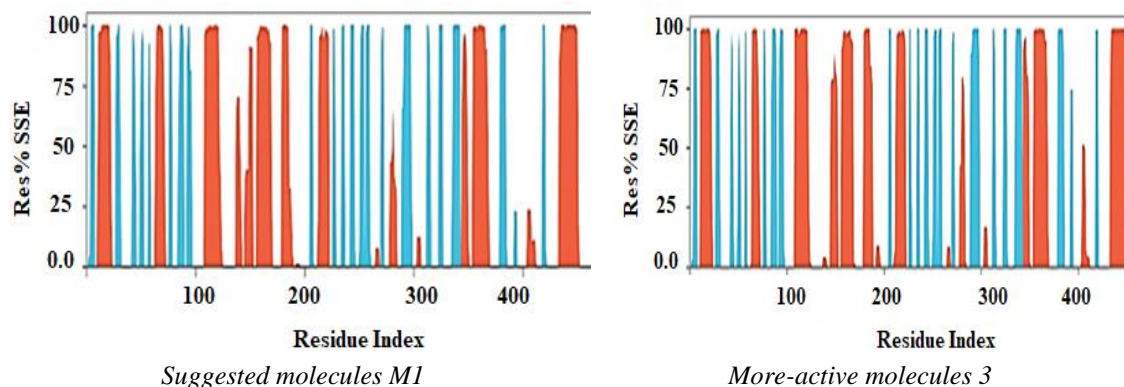


Figure 11. Comparing Secondary Structure Compositions of complex M1 and complex 3 in Molecular Dynamics

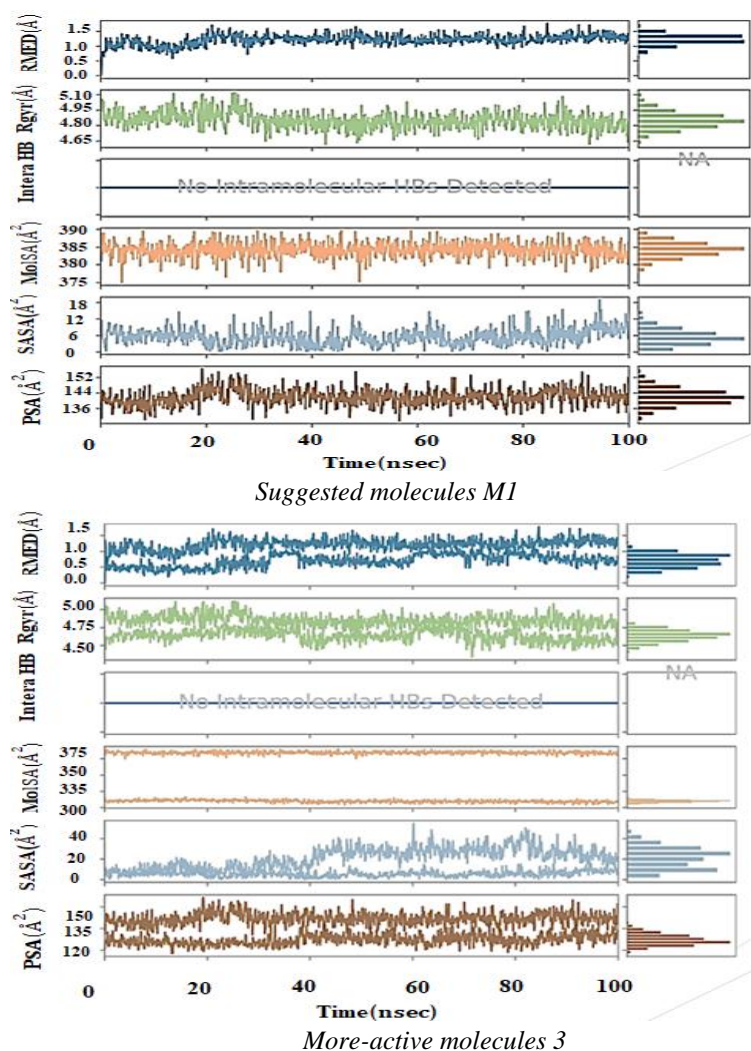


Figure 12. Comparing Structural Properties of the Proposed Molecule and the Most Active Molecule in Molecular Dynamics

The results of molecular dynamics reveal significant differences between the proposed molecule M1 and the most active molecule 3. For

the proposed molecule, RMSD varies between 0.5 and 1 angstrom, indicating relatively low structural fluctuations. Rg shows a variation between 4.65

Moulay Ahfid El Alaouy, Marwa Alaqarbeh, Mohamed Ouabane, Abdelouahid Sbai, Hamid Maghat, Tahar Lakhlifi, Mohammed Bouachrine

and 5.1 Å, suggesting some flexibility in molecular size. The absence of major intramolecular interactions indicates internal stability. The molecular surface area (MolSA) ranges from 375 to 390 Å², with a solid surface, while solvent-accessible surface area (SASA) varies from 0 to 18 Å², indicating some solvent exposure, and polar surface area (PSA) ranges from 136 to 152 Å², displaying polar regions.

On the other hand, for the most active molecule 3, RMSD varies between 0.3 and 1.5 Å, with a slightly broader range. Rg varies between 4.5 and 5 Å, indicating a slightly more compact size. The absence of significant intramolecular interactions also suggests internal stability. MolSA exhibits subtle variations, both between 300 and 325 Å² and between 375 and 400 Å², reflecting delicate changes in molecular surface. SASA varies from 0 to 40 Å², indicating variable solvent exposure, and PSA ranges from 136 to 158 Å², showing greater variability in polar regions.

In summary, these results suggest that the proposed molecule exhibits slightly more consistent stability with limited fluctuations compared to the most active molecule, which displays greater variability in some of its properties, potentially due to more significant conformational changes. These differences could have important implications for their respective biological behavior. These different properties are shown in (Fig. 12).

3.8. Retrosynthesis results

In this study, the retrosynthetic method was employed with the assistance of the Spaya platform to facilitate the creation of the target compound, namely methyl 3-{2-[(2E)-2-[1-(3-nitrothiophen-2-yl) but-3-en-1-ylidene] hydrazin-1-yl]-1,3-thiazol-4-yl}benzoate (referred to as M1), which represents a potential drug candidate as a selective inhibitor of human MAO-B. The analysis generated several synthesis options, among which the one with the highest score of 0.7 was selected. Therefore, the optimal synthesis route consisting of five steps was chosen. This approach is based on similar synthesis methods already described in the literature (details available in Table 12 and Figure 13).

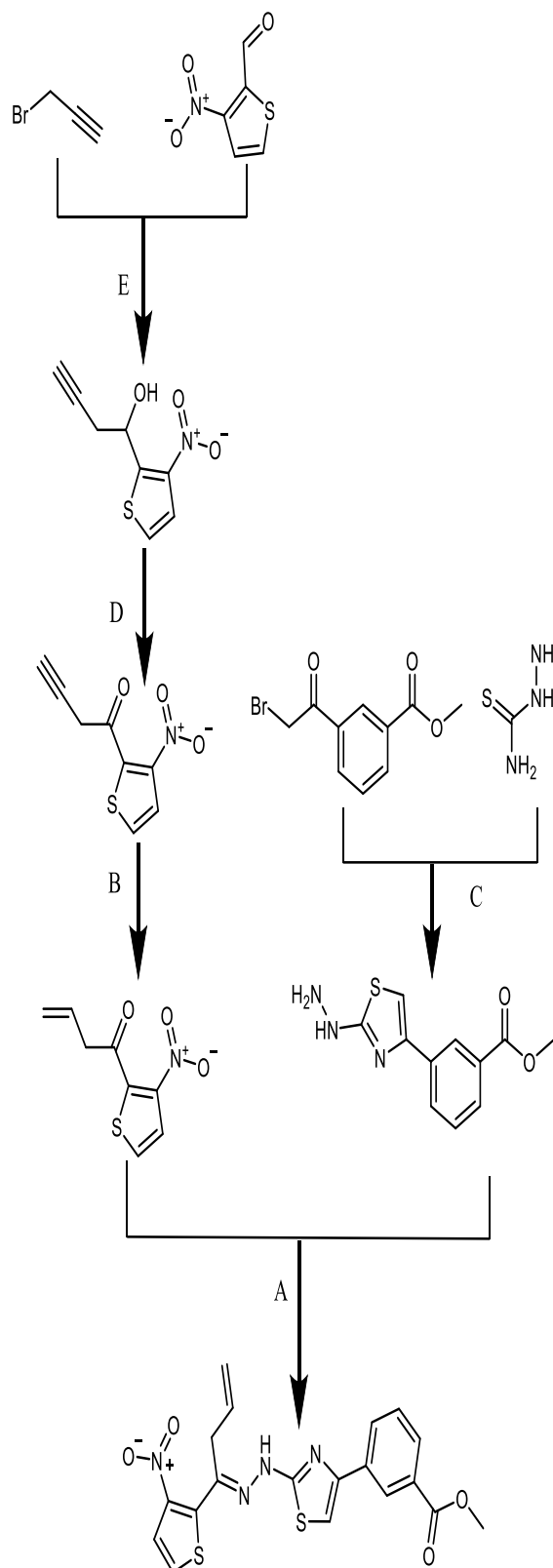
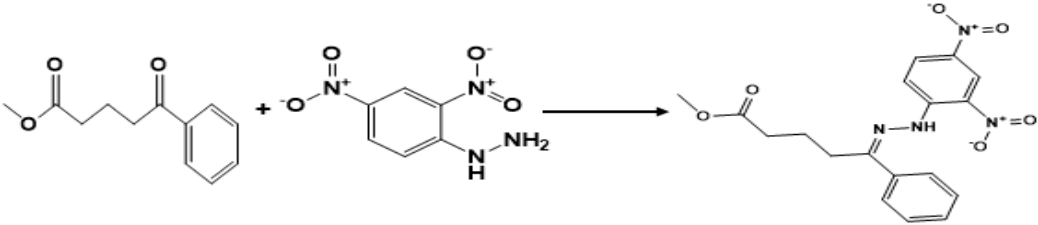
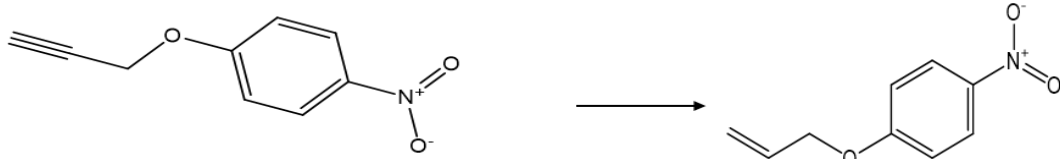
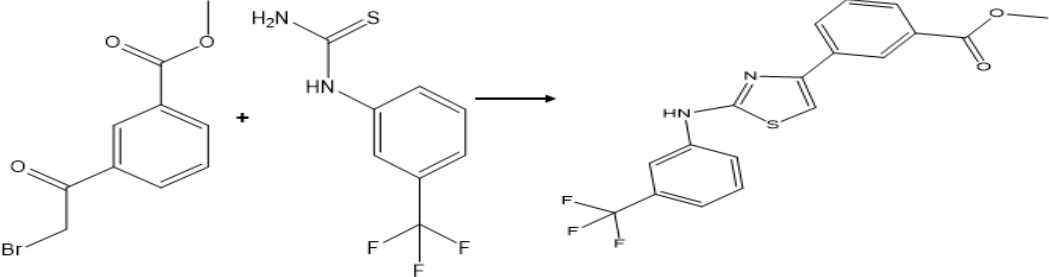
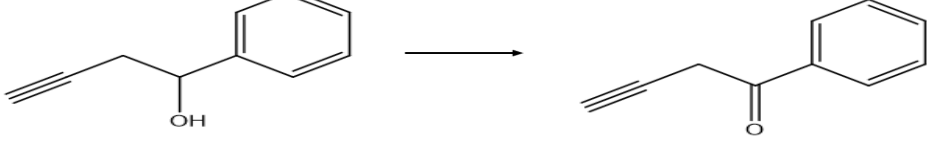
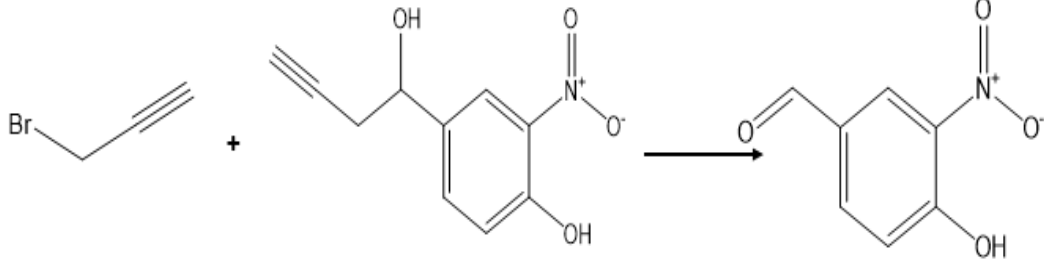


Figure 13. depicts the sequence of different stages generated subsequent to the analysis.

Moulay Ahfid El Alaouy, Marwa Alaqarbeh, Mohamed Ouabane, Abdelouahid Sbai, Hamid Maghat, Tahar Lakhli, Mohammed Bouachrine

Table 12. Reactions to be used as guidelines for synthesis of M1 drug candidate.

Steps	Similarity
Allen, Cressman Journal of the American Chemical Society, 1933, vol. 55, p. 2953,2958	
<p>A</p> 	0.22
Wesquet, Alexander O., Kazmaier, Uli Advanced Synthesis and Catalysis, 2009, vol. 351, # 9 p. 1395 - 1404	
<p>B</p> 	0.24
Thiazole synthesis, Reference: US11608329_C00606	
<p>C</p> 	0.57
Liu, Jinxian, Ma, Shengming Tetrahedron, 2013, vol. 69, # 47 p. 10161- 10167	
<p>D</p> 	0.28
Bromo aldehyde Barbier reaction, Reference:US20210023113A1_0147	
<p>E</p> 	0.38

[4] Conclusions

The study employed a Partial Least Squares (PLS) analysis to develop robust 3D-QSAR models capable of external predictions. The objective was to accurately predict new monoamine oxidase B (MAO-B) inhibitors with enhanced efficacy. To achieve this, it used a dataset consisting of derivatives of 4-(3-nitrophenyl) thiazole-2-ylhydrazone. The CoMSIA/SEA models were developed with excellent statistical results ($Q^2 =$

0.60 ; $R^2 = 0.97$; $R^2_{test} = 0.711$; $F = 151.84$; $SEE = 0.21$; $ONC = 4$), demonstrating their notable performance and strong predictive ability. These results were subjected to internal and external tests to validate the model, thereby enhancing its reliability. Contour maps generated by these models identified crucial structural features impacting inhibitory activity. Consequently, four new molecules (M1-M4) with predicted higher inhibitory activity were designed. Using the crystal

Moulay Ahfid El Alaouy, Marwa Alaqarbeh, Mohamed Ouabane, Abdelouahid Sbai, Hamid Maghat, Tahar Lakhliifi, Mohammed Bouachrine

structure of the hMAO-B protein, the analysis of interactions between the new compounds (M1-M4) and reference compound 3 revealed that all proposed molecules formed significant bonds with major and minor residues such as Arg:42, Glu:58, Met:436, Tyr:398, Tyr:435, and Tyr60. Moreover, more significant interactions than those observed in complex 3 were noted. These findings suggest that the complex with molecule M1 might exhibit increased stability towards the target protein compared to the complex formed with reference compound 3. Molecular docking results confirmed the conclusions of the 3D-QSAR study. ADMET predictions revealed that the newly created molecules (M1-M4) are likely to be orally bioavailable, displaying high gastrointestinal absorption (greater than 80%). Additionally, they acted as substrates and inhibitors of CYP3A4. Furthermore, these molecules demonstrated an absence of toxicity, except for reference compound 3, which exhibited persistent toxicity and did not show inhibition towards CYP3A4. Among the compounds studied, compound M1 stood out as one of the most promising candidates, displaying enhanced stability and increased affinity towards the active site of the MAO-B receptor compared to compound 3. Molecular dynamics (MD) simulations lasting 100 ns were conducted to assess the stability of the novel molecule M1 in comparison to the most active compound. The results of these MD simulations confirmed the stability of molecule M1. This was supported by the analysis of RMSD and RMSF values, interactions with the protein, as well as structural properties. Finally, a retrosynthetic approach was adopted to efficiently plan the synthesis of compound M1 as a potential MAO-B inhibitor. This study opens promising avenues for improving treatments for Parkinson's disease and other conditions related to MAO-B activity.

Authors' contributions

Moulay Ahfid El Alaouy: article writing, graph preparation, data analysis, and interpretation;
Marwa Alaqarbeh: paper writing, analyzed and interpreted molecular dynamic simulation data;
Abdelouahid Sbai, Hamid Maghat, Tahar Lakhliifi, and Mohammed Bouachrine: project review, editing, and supervision.

Availability of data and materials Not Applicable

Code availability There is no software code for this article.

Funding Not Applicable

Declarations

Ethical Approval Not applicable; no human or animal studies have been carried out.

Conflict of interest The authors declare no competing interests.

References

- [1] N. Özdemir, M. Dinçer, A. Çukurovalı, O. Büyükgüngör, Experimental and theoretical investigation of the molecular and electronic structure of 5-(4-aminophenyl)-4-(3-methyl-3-phenylcyclobutyl)thiazol-2-amine, *Journal of Molecular Modeling.*, 15 (2009) 1435–1445.
- [2] J. Jose, J.K. Varughese, M.K. Parvez, T.V. Mathew, Probing the inhibition of MAO-B by chalcones: an integrated approach combining molecular docking, ADME analysis, MD simulation, and MM-PBSA calculations, *Journal of Molecular Modeling.*, 30 (2024) 103.
- [3] V.L. Tananta, E.V. Costa, Y.S. Mary, Y.S. Mary, J. S.Al-Otaibi, R.A. Costa, DFT, ADME studies and evaluation of the binding with HSA and MAO-B inhibitory potential of protoberberine alkaloids from *Guatteria friesiana*: theoretical insights of promising candidates for the treatment of Parkinson's disease, *Journal of Molecular Modeling.*, 29 (2023) 353.
- [4] F.P. Moraes, W.F. De Azevedo, Targeting imidazoline site on monoamine oxidase B through molecular docking simulations, *Journal of Molecular Modeling.*, 18 (2012) 3877–3886.
- [5] M. D'Ascenzio, P. Chimenti, M.C. Gidaro, C. De Monte, D. De Vita, A. Granese, L. Scipione, R. Di Santo, G. Costa, S. Alcaro, M. Yáñez, S. Carradori, (Thiazol-2-yl)hydrazone derivatives from acetylpyridines as

Moulay Ahfid El Alaouy, Marwa Alaqarbeh, Mohamed Ouabane, Abdelouahid Sbai, Hamid Maghat, Tahar Lakhlifi, Mohammed Bouachrine

- dual inhibitors of MAO and AChE: synthesis, biological evaluation and molecular modeling studies, *Journal of Enzyme Inhibition and Medicinal Chemistry*, 30 (2015) 908–919.
- [6] Y.-Q. Zhu, J.-F. Pei, Z.-M. Liu, L.-H. Lai, J.-R. Cui, R.-T. Li, 3D-QSAR studies on tripeptide aldehyde inhibitors of proteasome using CoMFA and CoMSIA methods, *Bioorganic & Medicinal Chemistry*, 14 (2006) 1483–1496.
- [7] D. Secci, S. Carradori, A. Petzer, P. Guglielmi, M. D’Ascenzio, P. Chimenti, D. Bagetta, S. Alcaro, G. Zengin, J.P. Petzer, F. Ortuso, 4-(3-Nitrophenyl)thiazol-2-ylhydrazone derivatives as antioxidants and selective hMAO-B inhibitors: synthesis, biological activity and computational analysis, *Journal of Enzyme Inhibition and Medicinal Chemistry*, 34 (2019) 597–612.
- [8] T.R. Anderson, T.A. Slotkin, Maturation of the adrenal medulla-IV Effects of morphine, *Biochemical Pharmacology*, 24 (1975) 1469–1474.
- [9] A. Shibu, S. Jones, P.L. Tolley, D. Diaz, C.O. Kwiatkowski, D.S. Jones, J.M. Shivas, J.J. Foley, T.A. Schmedake, M.G. Walter, Correlating structure and photophysical properties in thiazolo[5,4-d]thiazole crystal derivatives for use in solid-state photonic and fluorescence-based optical devices, *Materials Advances*, 4 (2023) 6321–6332.
- [10] K. Ravi Singh, T.N. Lohith, T. Ananth Nag, M.A. Sridhar, M.P. Sadashiva, Structure property relationship in two thiazole derivatives: Insights of crystal structure, Hirshfeld surface, DFT, QTAIM, NBO and molecular docking studies, *Molecular Crystals and Liquid Crystals*, 763 (2023) 54–72.
- [11] H. Hadni, M. Elhallaoui, 3D-QSAR, docking and ADMET properties of aurone analogues as antimalarial agents, *Heliyon*, 6 (2020) e03580.
- [12] M.A. El Alaouy, M. Alaqarbeh, M. Ouabane, H. Zaki, M. ElBouhi, H. Badaoui, Y. Moukhliiss, A. Sbai, H. Maghat, T. Lakhlifi, M. Bouachrine, Computational Prediction of 3,5-Diaryl-1H-Pyrazole and spiropyrazolines derivatives as potential acetylcholinesterase inhibitors for alzheimer disease treatment by 3D-QSAR, molecular docking, molecular dynamics simulation, and ADME-Tox, *Journal of Biomolecular Structure and Dynamics*, (2023) 1–14.
- [13] D. Secci, S. Carradori, A. Petzer, P. Guglielmi, M. D’Ascenzio, P. Chimenti, D. Bagetta, S. Alcaro, G. Zengin, J.P. Petzer, F. Ortuso, 4-(3-Nitrophenyl)thiazol-2-ylhydrazone derivatives as antioxidants and selective hMAO-B inhibitors: synthesis, biological activity and computational analysis, *Journal of Enzyme Inhibition and Medicinal Chemistry*, 34 (2019) 597–612.
- [14] Y. Wang, F. Bai, H. Cao, J. Li, H. Liu, P. Gramatica, A Combined Quantitative Structure-Activity Relationship Research of Quinolinone Derivatives as Androgen Receptor Antagonists, *Combinatorial Chemistry & High Throughput Screening*, 18 (2015) 834–845.
- [15] C. Hansch, A. Kurup, R. Garg, H. Gao, Chem-Bioinformatics and QSAR: A Review of QSAR Lacking

Moulay Ahfid El Alaouy, Marwa Alaqarbeh, Mohamed Ouabane, Abdelouahid Sbai, Hamid Maghat, Tahar Lakhliifi, Mohammed Bouachrine

- Positive Hydrophobic Terms, Chemical Reviews., 101 (2001) 619–672.
- [16] M. Shahlaei, A. Fassihi, L. Saghaie, E. Arkan, A. Madadkar-Sobhani, A. Pourhossein, Computational evaluation of some indenopyrazole derivatives as anticancer compounds; application of QSAR and docking methodologies, Journal of Enzyme Inhibition and Medicinal Chemistry., 28 (2013) 16–32.
- [17] M. Boutalaka, S. El Bahi, M. Alaqarbeh, M.A. El Alaouy, Y. Koubi, K.E. Khatabi, H. Maghat, M. Bouachrine, T. Lakhliifi, Computational investigation of imidazo[2,1-b]oxazole derivatives as potential mutant BRAF kinase inhibitors: 3D-QSAR, molecular docking, molecular dynamics simulation, and ADMETox studies, Journal of Biomolecular Structure and Dynamics., (2023) 1–20.
- [18] S. El Bahi, M. Boutalaka, M.A. El Alaouy, S. Bouamrane, M. Alaqarbeh, M. Choukrad, A. Sbai, M. Bouachrine, T. Lakhliifi, Computational investigation of novel pyrimidine derivatives as potent FAK inhibitors via 3D-QSAR, molecular docking, molecular dynamics simulation and retrosynthesis, New Journal of Chemistry., 47 (2023) 12816–12829.
- [19] K. Tabti, S. Baammi, L. ElMchichi, A. Sbai, H. Maghat, M. Bouachrine, T. Lakhliifi, Computational investigation of pyrrolidin derivatives as novel GPX4/MDM2–p53 inhibitors using 2D/3D-QSAR, ADME/toxicity, molecular docking, molecular dynamics simulations, and MM-GBSA free energy, Journal of Structural Chemistry., 33 (2022) 1019–1039.
- [20] H.T.T. Lai, L.H. Nguyen, A.D. Phan, A. Kranjc, T.T. Nguyen, D. Nguyen-Manh, A comparative study of receptor interactions between SARS-CoV and SARS-CoV-2 from molecular modeling, Journal of Molecular Modeling., 28 (2022) 305.
- [21] M.A. El Alaouy, M. Alaqarbeh, M. Ouabane, H. Zaki, M. ElBouhi, H. Badaoui, Y. Moukhliiss, A. Sbai, H. Maghat, T. Lakhliifi, M. Bouachrine, Computational Prediction of 3,5-Diaryl-1H-Pyrazole and spiropyrazolines derivatives as potential acetylcholinesterase inhibitors for alzheimer disease treatment by 3D-QSAR, molecular docking, molecular dynamics simulation, and ADME-Tox, Journal of Biomolecular Structure and Dynamics., (2023) 1–14.
- [22] R. Mahmoudzadeh Laki, E. Pourbasheer, 3D-QSAR Modeling on 2-Pyrimidine Carbohydrazides as Utrophin Modulators for the Treatment of Duchenne Muscular Dystrophy by Combining CoMFA, CoMSIA, and Molecular Docking Studies, ACS Omega Journal, 9 (2024) 24707–24720.
- [23] K.A. Saad, M.A. Eldawy, K.M. Elokely, Studies of the symmetric binding mode of daclatasvir and analogs using a new homology model of HCV NS5A GT-4a, Journal of Molecular Modeling., 29 (2023) 25.
- [24] S. Carradori, F. Ortuso, A. Petzer, D. Bagetta, C. De Monte, D. Secci, D. De Vita, P. Guglielmi, G. Zengin, A. Aktumsek, S. Alcaro, J.P. Petzer, Design, synthesis and biochemical evaluation of novel multi-target inhibitors as potential anti-Parkinson agents, European Journal of

Moulay Ahfid El Alaouy, Marwa Alaqarbeh, Mohamed Ouabane, Abdelouahid Sbai, Hamid Maghat, Tahar Lakhliifi, Mohammed Bouachrine

- Medicinal Chemistry., 143 (2018) 1543–1552.
- [25] X. Chai, J. Zhang, H. Hu, S. Yu, Q. Sun, Z. Dan, Y. Jiang, Q. Wu, Design, synthesis, and biological evaluation of novel triazole derivatives as inhibitors of cytochrome P450 14 α -demethylase, *European Journal of Medicinal Chemistry.*, 44 (2009) 1913–1920.
- [26] L. El Mchichi, A. El Aissouq, R. Kasmi, A. Belhassan, R. El-Mernissi, A. Ouammou, T. Lakhliifi, M. Bouachrine, In silico design of novel Pyrazole derivatives containing thiourea skeleton as anti-cancer agents using: 3D QSAR, Drug-Likeness studies, ADMET prediction and molecular docking, *Mater. Materials Today: Proceedings.*, 45 (2021) 7661–7674.
- [27] S. Bouamrane, A. Khaldan, H. Hajji, R. El-mernissi, M. Alaqarbeh, N. Alsakhen, H. Maghat, M.A. Ajana, A. Sbai, M. Bouachrine, T. Lakhliifi, In silico identification of 1,2,4-triazoles as potential *Candida Albicans* inhibitors using 3D-QSAR, molecular docking, molecular dynamics simulations, and ADMET profiling, *Molecular Diversity.*, 27 (2023) 2111–2132.
- [28] S. El Bahi, M. Boutalaka, M. Alaqarbeh, M.A. El Alaouy, Y. Koubi, K. El Khatabi, M. 'barek Choukrad, A. Sbai, M. Bouachrine, T. Lakhliifi, In-Silico Investigation of Osimertinib Based Compounds as Potential Double Mutant EGFR Kinase Inhibitors Against H1975 Cell Line: Integrating QSAR Modeling, Molecular Docking, MD Simulations, and ADME/Tox Studies, *Chemistry Africa.*, (2023).
- [29] Y.-K. Jiang, Molecular docking and 3D-QSAR studies on β -phenylalanine derivatives as dipeptidyl peptidase IV inhibitors, *Journal of Molecular Modeling.*, 16 (2010) 1239–1249.
- [30] Y. Liu, M. Grimm, W. Dai, M. Hou, Z.-X. Xiao, Y. Cao, CB-Dock: a web server for cavity detection-guided protein–ligand blind docking, *Acta Pharmacologica Sinica.*, 41 (2020) 138–144.
- [31] W. Li, Y. Tang, Y.-L. Zheng, Z.-B. Qiu, Molecular modeling and 3D-QSAR studies of indolomorphinan derivatives as kappa opioid antagonists, *Bioorganic & Medicinal Chemistry.*, 14 (2006) 601–610.
- [32] M.A. El Alaouy, S. El Bahi, M. Boutalaka, M. Ouabane, A. Sbai, H. Maghat, M. Bouachrine, T. Lakhliifi, Organic compounds based on 1-(prop-2-yn-1-ylamino)-2,3-dihydro-1H-indene-4-thiol as selective human monoamine oxidase B inhibitors Quantitative analysis of structure-activity relationships and in-silico investigations, *Moroccan Journal of Chemistry*, Vol. 11 (2023) *Mor. J. Chem.* 11 N°3 (2023) 802-817 Pages.
- [33] M. Stitou, H. Toufik, M. Bouachrine, F. Lamchouri, Quantitative structure–activity relationships analysis, homology modeling, docking and molecular dynamics studies of triterpenoid saponins as Kirsten rat sarcoma inhibitors, *Journal of Biomolecular Structure and Dynamics.*, 39 (2021) 152–170.
- [34] H. Zhao, D. Wei, M. Li, Y. Du, Substituent contribution to the genotoxicity of benzophenone-type UV filters, *Ecotoxicology and*

Moulay Ahfid El Alaouy, Marwa Alaqarbeh, Mohamed Ouabane, Abdelouahid Sbai, Hamid Maghat, Tahar Lakhlifi, Mohammed Bouachrine

- Environmental Safety., 95 (2013) 241–246.
- [35] S. Elbahi, Y. Koubi, M. Boutalaka, H. Hajji, M. Chokrad, M.A. Ajana, T. Lakhlifi, The c-Src kinase inhibitors: 2D-QSAR study by Multiple Linear Regression method, RHAZES: Green and Applied Chemistry., (2021) 29-42 Pages.
- [36] E. Edache, A. UzaiRu, P.A. Mamza, G.A. Shallangwa, Molecular phylogeny, Sequence-based drug design, Docking built virtual screening, dynamics simulations, and ADMET properties of thiazolino 2-pyridone amide derivatives as an inhibitor of Chlamydia trachomatis and SARS-CoV-2 protein, Turkish Computational and Theoretical Chemistry., 8 (2024) 10–39.
- [37] A. SaviOur, G.A. Shallangwa, A. UzaiRu, In Silico study for investigating and predicting the activities of 7-Hydroxy-1,3-dioxo-2,3-dihydro-1H-pyrrolo[3,4-c]pyridine-4-carboxylate Derivatives as Potent Anti-HIV Agents, Turkish Computational and Theoretical Chemistry., 4 (2020) 49–58.
- [38] Y. Hasan, A. Al-hamashi, Identification of Selisistat Derivatives as SIRT1-3 Inhibitors by in Silico Virtual Screening, Turkish Computational and Theoretical Chemistry., 8 (2024) 1–11.
- [39] İ. MomohjiMoh Ovaku, A. Stephehe EyiJe, S. GiDeon Adamu, U. Adamu, QSAR and Molecular Docking Studies of novel thiophene, pyrimidine, coumarin, pyrazole and pyridine derivatives as Potential Anti-Breast Cancer Agent, Turkish Computational and Theoretical Chemistry., 4 (2020) 12–23.
- [40] S. Elijah, S. Uba, A. Uzairu, MULTIVARIANT QSAR MODEL FOR SOME POTENT COMPOUNDS AS POTENTIAL ANTI-TUMOR INHIBITORS: A COMPUTATIONAL APPROACH, Turkish Computational and Theoretical Chemistry., 3 (2019) 38–46.
- [41] J. Shi, L.-X. Zhao, J.-Y. Wang, T. Ye, M. Wang, S. Gao, F. Ye, Y. Fu, The novel 4-hydroxyphenylpyruvate dioxygenase inhibitors in vivo and in silico approach: 3D-QSAR analysis, molecular docking, bioassay and molecular dynamics, Arabian Journal of Chemistry., 15 (2022) 103919.
- [42] L. Dahiya, M.K. Mahapatra, R. Kaur, V. Kumar, M. Kumar, Validation of TZD Scaffold as Potential ARIs: Pharmacophore Modeling, Atom-based 3D QSAR and Docking Studies, Combinatorial Chemistry & High Throughput Screening., 20 (2017).
- [43] M. Rehan, O.S. Bajouh, Virtual screening of naphthoquinone analogs for potent inhibitors against the cancer-signaling PI3K/AKT/mTOR pathway, Journal of Cellular Biochemistry., 120 (2019) 1328–1339.
- [44] M.A.E. Alaouy, M. Alaqarbeh, S.E. Bahi, M. Boutalaka, S. Esslali, A. Sbai, H. Maghat, F. Guenoun, M. Choukrad, T. Lakhlifi, M. Bouachrine, Computational Prediction of Spiropyrazoline Derivatives as Potential Acetylcholinesterase Inhibitors for Alzheimer's Disease Treatment, Russian Journal of Bioorganic Chemistry., 50 (2024) 1016–1036.

Moulay Ahfid El Alaouy, Marwa Alaqarbeh, Mohamed Ouabane, Abdelouahid Sbai, Hamid Maghat, Tahar Lakhli, Mohammed Bouachrine

- [45] O. Trott, A.J. Olson, AutoDock Vina: Improving the speed and accuracy of docking with a new scoring function, efficient optimization, and multithreading, *Journal of Computational Chemistry.*, 31 (2010) 455–461.
- [46] M. De Vivo, M. Masetti, G. Bottegoni, A. Cavalli, Role of Molecular Dynamics and Related Methods in Drug Discovery, *Journal of Medicinal Chemistry.*, 59 (2016) 4035–4061.
- [47] D. Secci, S. Carradori, B. Bizzarri, P. Chimenti, C. De Monte, A. Mollica, D. Rivanera, A. Zicari, E. Mari, G. Zengin, A. Aktumsek, Novel 1,3-thiazolidin-4-one derivatives as promising anti- *Candida* agents endowed with anti-oxidant and chelating properties, *European Journal of Medicinal Chemistry.*, 117 (2016) 144–156.
- [48] B. Rosada, A. Bekier, J. Cytarska, W. Płaziński, O. Zavyalova, A. Sikora, K. Dzitko, K.Z. Łączkowski, Benzo[b]thiophene-thiazoles as potent anti-*Toxoplasma gondii* agents: Design, synthesis, tyrosinase/tyrosine hydroxylase inhibitors, molecular docking study, and antioxidant activity, *European Journal of Medicinal Chemistry.*, 184 (2019) 111765.
- [49] S.J. Ansari, S. Kundu, S. Mogurampelly, Molecular dynamics simulations of the effect of starch on transport of water and ions through graphene nanopores, *Journal of Molecular Modeling.*, 30 (2024) 125.
- [50] Z. Lou, C. Cheng, Y. Cui, H. Tian, Interfacial interaction–driven rheological properties of quartz nanofluids from molecular dynamics simulations and density functional theory calculations, *Journal of Molecular Modeling.*, 28 (2022) 189.
- [51] P.F.J. Lipiński, M. Jarończyk, J.Cz. Dobrowolski, J. Sadlej, Molecular dynamics of fentanyl bound to μ -opioid receptor, *Journal of Molecular Modeling.*, 25 (2019) 144.